MATHEMATICAL ANALYSIS OF RESONANCES FOR AN ARRAY OF SUBWAVELENGTH ANNULAR HOLES AND ITS APPLICATION IN SUPER-RESOLUTION IMAGING

JIAXIN ZHOU*, JUNSHAN LIN†, WANGTAO LU‡, AND HAI ZHANG§

Abstract. This work presents a mathematical analysis of resonances for an array of subwavelength coaxial annular holes and a new super-resolution imaging approach using the resonant structure. By employing a multiscale analytical framework based on a combination of the integral equation in the exterior domain and the waveguide mode expansion inside the small three-dimensional holes, we derive asymptotic expansions of complex-valued scattering resonances for the underlying subwavelength structure and analyze the electromagnetic field amplification at the resonant frequencies. In particular, it is shown that the resonant modes oscillate on a subwavelength scale in the near field if the annular holes are placed close to each other. By leveraging this observation, we develop a novel super-resolution imaging approach that utilizes resonant modes through the subwavelength resonant structure as the illuminate pattern and present a numerical reconstruction algorithm to solve the underlying inverse problem. Numerical examples show that a ten-fold improvement can be achieved in image resolution with the new imaging method.

Key words. Maxwell's equations, scattering resonances, super-resolution imaging

MSC codes. 35B34, 35Q61, 78A46

1. Introduction.

1.1. Background and motivation. The resonant scattering through subwavelength holes has attracted significant research interest since the seminal work [14] on so-called extraordinary optical transmission (EOT). Various subwavelenth hole structures have been developed for applications in biological sensing, near-field spectroscopy, and novel optical device design [38]. Mathematically there has been significant progress in analyzing the resonances for subwavelength hole structures. We refer the readers to [3, 15, 21, 30, 40, 27, 34] for the analysis of the scattering resonance through a finite number of subwavelength slit or circular holes and [7, 29, 31, 32] for resonances through an infinite periodic array of subwavelength slit holes in the setting of scalar wave equation. Therein either the integral equation or the mode matching methods are developed to study the resonances and the induced EOT phenomenon through the small holes. More recently, the resonances for the three-dimensional electromagnetic scattering was first investigated in [28] for an annular subwavelenth hole, in which a multiscale analysis framework was developed by combining the waveguide mode expansion in the tiny hole and the Stratton-Chew formula in the exterior of the hole.

In this work, we explore the electromagentic wave scattering resonances through

*Liu Bie Ju Centre for Mathematical Sciences, CityU of HK, Kowloon, Hong Kong (jiaxzhou@cityu.edu.hk).

†Department of Mathematics and Statistics, Auburn University, Auburn, AL 36849 (jzl0097@auburn.edu). JL is partially supported by NSF grant DMS-2410645.

‡School of Mathematical Sciences, Zhejiang University, Hangzhou 310027, China (wangtaolu@zju.edu.cn). WL is partially supported by the National Key Research and Development Program of China (2024YFA1012600, 2023YFA1009100), China NSF grant 12174310, and a Key Project of Joint Funds for Regional Innovation and Development (U21A20425), Zhejiang Provincial NSF Distinguished Youth Program (Extended Program RG25A010002).

§Department of Mathematics, HKUST, Clear Water Bay, Kowloon, Hong Kong (haizhang@ust.hk). HZ was partially supported by Hong Kong RGC grant GRF 16304621 and NSFC grant 12371425.

an array of subwavelength annular holes and develop a super-resolution imaging method by using the resonant structure. In optical imaging, super-resolution refers to imaging objects with a resolution beyond the Rayleigh diffraction limit, and the research in this field has witnessed significant progress in the past two decades [22]. Generally speaking, the resolution of the wave-based imaging is limited by the spatial frequency of the illumination or diffraction wave [22]. As such the image resolution can be improved by near-field techniques that probe the samples or collect the diffracted optical field in the vicinity of the object to get access to the evanescent wave [17, 19, 37], or the structured illumination approaches that use high spatial frequency wave pattern so as to shrink the support of point spread function [16, 20]. While the former can improve the resolution of images significantly, the major challenge lies in controlling the distance of the probe over the sample surface with extremely high precision. The latter does not require controlling the probe-sample distance, but the improvement of the resolution is less significant. Mathematically, the inverse scattering theory can be applied to understand how the structure of an imaging sample is encoded in the optical signal; see [4, 5, 8, 9, 10] for the related studies in several near-field imaging modalities.

In this work, by analyzing the resonances for an array of annular holes and the electromagnetic field pattern at the resonant frequencies, we show that the significantly amplified wave field through the tiny holes attains high spatial frequency along the horizontal direction when the annular holes are placed close to each other. Based on such observation, we propose to use the highly oscillatory resonant modes of the subwavelength structure as an illumination pattern for imaging, which allows for probing the high spatial-frequency information of the imaging sample. The inversion process is formulated as an inverse scattering problem of reconstructing the medium coefficient from the collected far-field data. The method leads to a significant improvement of the image resolution when the inverse problem is solved in a stable manner numerically to decode the high-frequency component of the imaging sample from the low spatial-frequency far field. The super-resolution approach presented in this work is inspired by a series of works in [24, 25, 26], where subwavelength resonators are used to achieve super-focusing, a key ingredient for super-resolution imaging; See also [1, 2] for the related mathematical theory. Finally, we refer to [33] for super-resolution imaging in 2D resonant structure, wherein the resonant modes from an array of slit holes are used as illumination patterns.

1.2. Subwavelength annular structure and resonant scattering. We consider an array of P coaxial annular holes that are patterned in a metallic slab of thickness l. The top and side views of the subwavelength structure are depicted in Figure 1(a) and 1(b), respectively. The annular holes occupy the domain $G^h = R^h \times (-l/2, l/2)$, where

$$R^h := \cup_{p=1}^{P} R_p^{h_p}, \quad R_p^{h_p} := \{(x_1, x_2) \in \mathbb{R}^2 : a_p < (x_1^2 + x_2^2)^{1/2} < a_p(1 + h_p)\}. \tag{1.1}$$

In the above, $R_p^{h_p}$ denotes the cross-sectional annulus on the x_1x_2 plane with inner and outer radii $\{a_p\}$ and $\{a_p(1 + h_p)\}$ respectively. Here and henceforth, we assume $a_1 < a_2 < \ldots < a_P$ and $h_p < h \ll l$. The domain occupied by the metallic structure is denoted by $\Omega_M := \{(x_1, x_2, x_3) \in \mathbb{R}^3 : (x_1, x_2) \in \mathbb{R}^2 \backslash \overline{R^h}, x_3 \in (-l/2, l/2)\}$.

Let the annular holes be filled with homogeneous non-magnetic materials. The electric permittivity function $\epsilon(x)$ takes the value $\epsilon = \epsilon_0$ above and below the metal, and $\epsilon = \epsilon_1$ in each annular hole. We denote the magnetic permeability in the vacuum

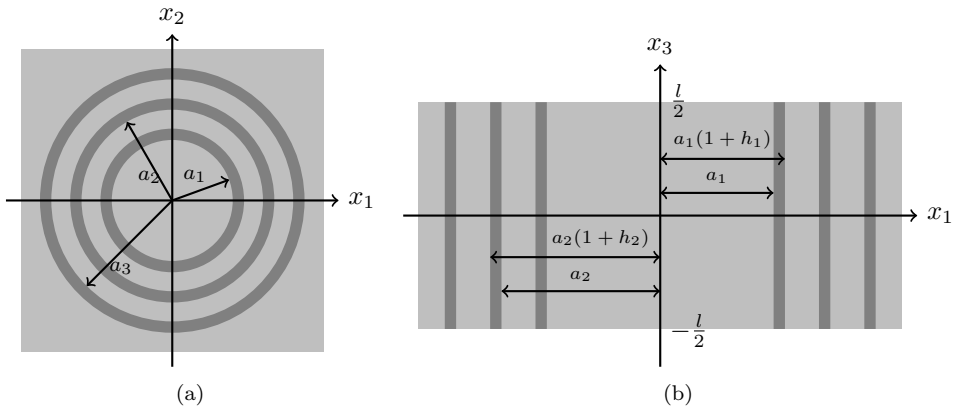

FIG. 1. *A PEC slab of thickness l with P coaxial subwavelength annular holes $\{G_p^{h_p}\}_{p=1}^P$ filled with homogeneous medium: (a) a top view; (b) a side view. These holes possess annular apertures $\{R_p^{h_p}\}_{p=1}^P$ on the x_1x_2 plane with inner and outer radii denoted by $\{a_p\}_{p=1}^P$ and $\{a_p(1+h_p)\}_{p=1}^P$ respectively.*

by μ_0. Let $k = \omega\sqrt{\mu_0\epsilon_0}$ be the free-space wavenumber. We consider the electromagnetic scattering by a plane wave $(\mathbf{E}^{\rm inc}, \mathbf{H}^{\rm inc})$. Then the total field $(\mathbf{E}^{\rm tot}, \mathbf{H}^{\rm tot})$, which consists of the incident plane wave, the reflected plane wave by the flat slab without holes, and the scattered waves $(\mathbf{E}^{\rm sca}, \mathbf{H}^{\rm sca})$, satisfies the following time-harmonic Maxwell equations in the domain $\mathbb{R}^3\backslash\overline{\Omega}_M$:

$$\text{curl } \mathbf{E}^{\rm tot} = \mathbf{i}\omega\mu_0\mathbf{H}^{\rm tot}, \tag{1.2}$$

$$\text{curl } \mathbf{H}^{\rm tot} = -\mathbf{i}\omega\epsilon\mathbf{E}^{\rm tot}, \tag{1.3}$$

The total electric field $\mathbf{E}^{\rm tot}$ satisfies the perfect electric conducting (PEC) boundary conditions on the metal surface $\partial\Omega_M$:

$$\boldsymbol{\nu} \times \mathbf{E}^{\rm tot} = 0, \tag{1.4}$$

where $\boldsymbol{\nu}$ denotes the outward unit normal. In addition, the Silver-Müller radiation condition is imposed at infinity above and below the metal (cf. [23]) for the scattered field:

$$\lim_{|\mathbf{x}|\to\infty} [\sqrt{\mu_0}\mathbf{H}^{\rm sca}(\mathbf{x}) \times \mathbf{x} - |\mathbf{x}|\sqrt{\epsilon_0}\mathbf{E}^{\rm sca}(\mathbf{x})] = 0. \tag{1.5}$$

To study the resonances, we begin by examining non-trivial solutions to the homogeneous problem for the above scattering problem when the incident wave is absent. Our first main result, detailed in Theorem 3.5, provides the asymptotic expansions of the complex-valued resonances for the scattering problem. When the incident wave is applied, the asymptotic expansion of the electromagnetic field at resonant frequencies is given in Theorem 3.6, which highlights the $O(1/h)$ amplification order for the electromagnetic field within and near the annular holes.

1.3. Super-resolution imaging method. The new super-resolution imaging method uses the resonant scattering of the coaxial annular holes discussed in Section 1.2. Figure 2 illustrates the imaging setup, where the sample is placed on the substrate that sits on top of the subwavelength structure. We arrange multiple holes within one

wavelength such that $a_P < \lambda$. The sample is non-magnetic and it possesses the permittivity function $\epsilon = (1 + q(\mathbf{x}))\epsilon_0$, wherein $q(\mathbf{x}) > 0$ is a bounded, real, and compactly supported function.

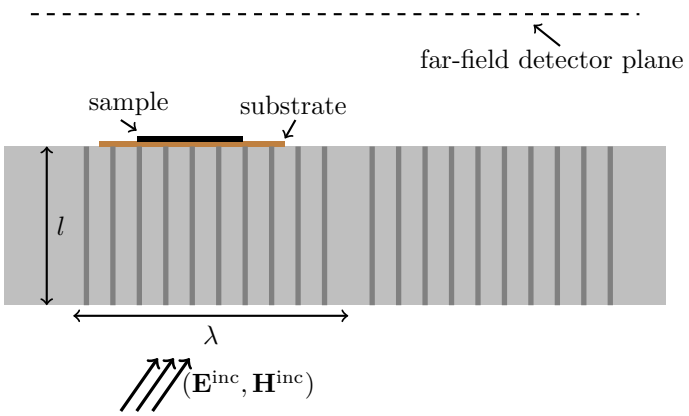

FIG. 2. *An incident field of wavelength $\lambda \approx a_P$ is applied below an infinite PEC metal of thickness l with many coaxial annular holes filled with homogeneous medium. The substrate and sample are placed just above the metal, and the scattered field is collected on the far-field detector plane.*

When an incident plane wave is illuminated from below at a resonant frequency, it triggers resonances across all annular holes. The corresponding transmitted signal is strong and it oscillates on a subwavelength scale along the horizontal direction. When the transmitted wave interacts with the imaging sample, it generates scattered field that propagates to the far-field detector plane. The key features of the imaging method are highlighted as follows:

(i) The oscillating transmitted wave generated by the resonant modes effectively probes the high spatial-frequency components of the sample. After interacting with the sample, they convert such information to the lower spatial-frequency components of the wave field, which propagates to the far-field.

(ii) The image of the sample is obtained by solving the inverse scattering problem of reconstructing $q(\mathbf{x})$ from the collected electric field $\mathbf{E}$ in the far-field. We employ a robust numerical algorithm to solve the inverse problem, and the inversion is stable by only using the low spatial-frequency components of the far-field data.

(iii) Super-resolution is obtained for the reconstructed image because the high spatial-frequency components of the sample are recovered through the inversion process. In particular, numerical examples show that a resolution with 1/20 of the wavelength can be achieved when $P = 10$.

(iv) The field enhancement induced by the resonant modes improves the signal-to-noise ratio and the robustness of the imaging approach.

2. Preliminaries.

2.1. Function spaces and notation. We introduce several Sobolev spaces of vector-valued functions used throughout the paper and refer the readers to [12, 23] for more details.

Let $\Omega \subset \mathbb{R}^3$ be a bounded Lipschitz domain and $\boldsymbol{\nu}(x)$ be the unit outward normal

on $\partial\Omega$. We define

$$H(\mathrm{curl},\Omega) :=\{\mathbf{F}\in[L^2(\Omega)]^3 : \mathrm{curl}\mathbf{F}\in[L^2(\Omega)]^3\},$$
$$H_t^s(\partial\Omega) :=\{\mathbf{F}\in[H^s(\partial\Omega)]^3 : \boldsymbol{\nu}\cdot\mathbf{F}=0\},\ -1/2\le s\le 1/2,$$
$$H^{-1/2}(\mathrm{Div},\partial\Omega) :=\{\mathbf{F}\in H_t^{-1/2}(\partial\Omega) : \mathrm{Div}\mathbf{F}\in H^{-1/2}(\partial\Omega)\},$$
$$H^{-1/2}(\mathrm{Curl},\partial\Omega) :=\{\mathbf{F}\in H_t^{-1/2}(\partial\Omega) : \mathrm{Curl}\mathbf{F}\in H^{-1/2}(\partial\Omega)\},$$

where Curl and Div denote the surface divergence and surface curl respectively (cf. (6.37) and (6.41) in [12]), which on the x_1x_2-plane can be written as

$$\mathrm{Div}=\nabla_2\cdot=[\partial_{x_1},\partial_{x_2}]\cdot,\ \mathrm{Curl}=\mathrm{curl}_2\cdot=[\partial_{x_2},-\partial_{x_1}]\cdot$$

For any $\mathbf{u}\in H(\mathrm{curl},\Omega)$, by the Theorem 5.24 in [23], we define two trace operators:

$$\gamma_t : H(\mathrm{curl},\Omega)\to H^{-1/2}(\mathrm{Div},\partial\Omega),\ \mathbf{u}\to\boldsymbol{\nu}\times\mathbf{u}|_{\partial\Omega}, \tag{2.1}$$
$$\gamma_T : H(\mathrm{curl},\Omega)\to H^{-1/2}(\mathrm{Curl},\partial\Omega),\ \mathbf{u}\to(\boldsymbol{\nu}\times\mathbf{u}|_{\partial\Omega})\times\boldsymbol{\nu}. \tag{2.2}$$

The spaces $H^{-1/2}(\mathrm{Div},\partial\Omega)$ and $H^{-1/2}(\mathrm{Curl},\partial\Omega)$ are dual spaces of each other, where the corresponding sesquilinear form can be defined as: $\forall\mathbf{f},\mathbf{g}\in H(\mathrm{curl},\Omega)$ s.t. $\mathbf{F}=\gamma_T(\mathbf{f}),\ \mathbf{G}=\gamma_t(\mathbf{g})$, we have

$$(\mathbf{F},\mathbf{G}) := -\int_\Omega \mathbf{f}\cdot\mathrm{curl}\overline{\mathbf{g}}-\mathrm{curl}\mathbf{f}\cdot\overline{\mathbf{g}}dx. \tag{2.3}$$

In the case $\Gamma\subset\partial\Omega$ is an open subset, we define

$$H^{-1/2}(\mathrm{Curl},\Gamma) := \{\mathbf{F}|_\Gamma : \mathbf{F}\in H^{-1/2}(\mathrm{Curl},\partial\Omega)\}, \tag{2.4}$$

and its dual space

$$\widetilde{H}^{-1/2}(\mathrm{Div},\Gamma) := \{\mathbf{F}\in H^{-1/2}(\mathrm{Div},\partial\Omega) : \mathrm{supp}\mathbf{F}\subset\overline{\Gamma}\}. \tag{2.5}$$

We also introduce the following notation:

(1). For any vector $\mathbf{V}=(V_1,V_2,V_3)\in\mathbb{C}^3$, we denote $\mathbf{V}^*$ by $\mathbf{V}^*=(V_1,V_2,-V_3)$. For any matrix $\mathbf{G}=(G_1,G_2,G_3)\in\mathbb{C}^{3\times3}$, we denote $\mathbf{G}^*=(G_1,G_2,-G_3)$;

(2). $\mathbb{R}^3_+ := \{\mathbf{x}\in\mathbb{R}^3 : x_3>l/2\}$: the half-space above the metal;

(3). $G_p^{h_p} := R_p^{h_p}\times(-l/2,l/2)$: the domain of the annular hole; $G_{+,p}^{h_p} := \{\mathbf{x}\in G_p^{h_p} : x_3>0\}$: the upper half of the annular hole $G_p^{h_p}$; $G_+^h := \cup_{p=1}^P G_{+,p}^{h_p}$.

(4). $A_p^{h_p}=\{\mathbf{x} : (x_1,x_2)\in R_p^{h_p}, x_3=l/2\}$: the upper annular aperture of $G_p^{h_p}$. And $A^h := \cup_{p=1}^P A_p^{h_p}$;

(5.) For $1\le p\le P$, we denote

$$\mathcal{X}_p(\mathbf{x}) = \begin{cases} 1, & \text{if } \mathbf{x}\in A_p^{h_p};\\ 0, & \text{otherwise.}\end{cases}$$

(6). $\mathcal{B} := \{z\in\mathbb{C} : |z|\le C_0\}$, where C_0 is a fixed positive constant;

(7). $\mathbb{N}^* := \mathbb{N}\backslash\{0\}$, and $(\mathbb{Z}\times\mathbb{N})^* := (\mathbb{Z}\times\mathbb{N})\backslash\{(0,0)\}$.

Finally, $A\lesssim B$ implies $A\le cB$ for some positive constant c.

2.2. Helmholtz decomposition and eigen-decomposition in a 2D domain . We first introduce the Helmholtz decomposition for vector fields defined in a 2D domain.

LEMMA 2.1 (Corollary 5′ in the Chapter IX of [13]). *Let $R \subset \mathbb{R}^2$ be a multiply connected and bounded C^2 domain and $\{\partial R_i\}$ denote all the connected components of ∂R, and then*

$$[L^2(R)]^2 = \nabla_2 H_0^1(R) \oplus \mathrm{curl}_2 H^1(R) \oplus \nabla_2 \mathbb{H}_2^1(R), \tag{2.6}$$

where $\mathbb{H}_2^1(R) := \{\phi : \ \phi \in H^1(R),\ \Delta_2\phi = 0,\ \phi|_{\partial R_i} = \text{constant for each } \partial R_i\}$ is of finite dimensions.

We then introduce eigen-decomposition for vector field defined on R. To this end, we introduce the Dirichlet and Neumann eigenpairs over R.

(1) $\{(\lambda_\tau^D, \psi_\tau^D)\}$ denote the set of all eigenpairs satisfying

$$\Delta_2\psi + \lambda\psi = 0, \text{ in } R, \tag{2.7}$$

$$\psi = 0, \text{ on } \partial R, \tag{2.8}$$

where $\left\{\frac{\nabla_2\psi_\tau^D}{\sqrt{\lambda_\tau^D}}\right\}$ is an orthonormal basis in $\nabla_2 H_0^1(R)$.

(2) $\{(\lambda_\eta^N, \psi_\eta^N)\}$ denote the set of all eigenpairs satisfying

$$\Delta_2\psi + \lambda\psi = 0,\ \lambda \neq 0, \text{in } R, \tag{2.9}$$

$$\partial_{\boldsymbol{\nu}}\psi = 0,\ \text{on } \partial R, \tag{2.10}$$

where $\left\{\frac{\mathrm{curl}_2\psi_\eta^N}{\sqrt{\lambda_\eta^N}}\right\}$ is an orthonormal basis in $\mathrm{curl}_2 H^1(R)$.

We also denote $\{\nabla_2\psi_\zeta^L\}$ as an orthonormal basis for $\nabla_2\mathbb{H}_2^1(R)$.

LEMMA 2.2. *For given $\mathbf{F}$ in $\widetilde{H}^{-1/2}(\mathrm{Div}, R)$ or $H^{-1/2}(\mathrm{Curl}, R)$, the following expansion converges:*

$$\begin{aligned}\mathbf{F} = &\sum_\tau \frac{1}{\lambda_\tau^D}[\mathrm{curl}_2\psi_\tau^D, \mathbf{F}]\mathrm{curl}_2\psi_\tau^D + \sum_\eta \frac{1}{\lambda_\eta^N}[\nabla_2\psi_\eta^N, \mathbf{F}]\nabla_2\psi_\eta^N \\ &+ \sum_\zeta [\mathrm{curl}_2\psi_\zeta^L, \mathbf{F}]\mathrm{curl}_2\psi_\zeta^L,\end{aligned} \tag{2.11}$$

where $[\cdot, \mathbf{F}]$ denotes the inner product $(\cdot, \mathbf{F})$ or $(\mathbf{F}, \cdot)$ separately.

Proof. Letting $\mathcal{D}(\overline{R})$ denote $\{u = U|_R, \text{ for some } U \in C_{\mathrm{comp}}^\infty(\mathbb{R}^2)\}$, the expansion (2.11) can be verified for each $\mathbf{F}$ in the spaces $\left[C_{\mathrm{comp}}^\infty(R)\right]^2 \subset \widetilde{H}^{-1/2}(\mathrm{Div}, R)$ and $\left[\mathcal{D}(\overline{R})\right]^2 \subset H^{-1/2}(\mathrm{Curl}, R)$ separately. Since $\left[C_{\mathrm{comp}}^\infty(R)\right]^2$ is dense in $\widetilde{H}^{-1/2}(\mathrm{Div}, R)$ and $\left[\mathcal{D}(\overline{R})\right]^2$ is dense in $H^{-1/2}(\mathrm{Curl}, R)$, the rest of proof follows from the Banach-Steinhaus theorem (cf. [39]). ∎

2.3. Helmholtz decomposition in a 3D domain.

LEMMA 2.3. *For a given real function $A(\mathbf{x})$, if there exist $c_1, c_2 \in \mathbb{R}$ that $c_2 > A(\mathbf{x}) > c_1 > 0$, then*

$$[L^2(\Omega)]^3 = [L^2(\mathrm{div}_A 0, \Omega)]^3 \oplus \nabla H_0^1(\Omega), \tag{2.12}$$

where

$$[L^2(\mathrm{div}_A 0,\Omega)]^3 := \{\mathbf{g}\in[L^2(\Omega)]^3 : (A\mathbf{g},\nabla\phi)_{[L^2(\Omega)]^3}=0, \forall\phi\in H_0^1(D)\}.$$

Moreover, $\forall\mathbf{g}\in\nabla H_0^1(\Omega)$*, we have* $\gamma_t(\mathbf{g})=0$ on $\partial\Omega$*, and*

$$H_\Gamma(\mathrm{curl},\Omega) = H_\Gamma(\mathrm{curl},\mathrm{div}_A 0,\Omega)\oplus\nabla H_0^1(\Omega), \tag{2.13}$$

where

$$H_\Gamma(\mathrm{curl},\Omega) := \{\mathbf{g}\in H(\mathrm{curl},\Omega) : \gamma_t(\mathbf{g})\in[L^2(\partial\Omega]^2, \gamma_t(\mathbf{g})=0 \text{ on } \Gamma\},$$
$$H_\Gamma(\mathrm{curl},\mathrm{div}_A 0,\Omega) := \{\mathbf{g}\in H_\Gamma(\mathrm{curl},\Omega) : (A\mathbf{g},\nabla\phi)_{[L^2(\Omega)]^3}=0, \forall\phi\in H_0^1(\Omega)\}.$$

Proof. (2.12) follows from Theorem 4.23 in [23]. We only need to prove that $\mathbf{g}\in\nabla H_0^1(\Omega)$ implies $\gamma_t(\mathbf{g})=0$ on $\partial\Omega$, and then (2.13) is a direct result of (2.12). For any $\mathbf{f}\in H(\mathrm{curl},\Omega)$, $g\in H_0^1(\Omega)$ and $\mathbf{g}=\nabla g$, from the equation (2.3), we obtain

$$\begin{aligned}(\gamma_T(\mathbf{f}),\gamma_t(\mathbf{g})) &= \int_\Omega \mathbf{f}\mathrm{curl}\nabla\overline{g} - \mathrm{curl}\mathbf{f}\cdot\nabla\overline{g}dv\\ &= \int_\Omega \mathbf{f}\mathrm{curl}\nabla\overline{g}dv + \int_\Omega \nabla\cdot\mathrm{curl}\mathbf{f}\overline{g}dv - \int_{\partial\Omega}\boldsymbol{\nu}\cdot\mathbf{f}\overline{g}ds.\end{aligned}$$

Then the desired result follows from the fact that $\mathrm{curl}\nabla = 0$, $\nabla\cdot\mathrm{curl} = 0$ and $g|_{\partial\Omega}=0$. ∎

2.4. Mode decomposition in a 3D waveguide. We introduce the mode decomposition in a waveguide that occupies the domain $G = R\times(-l/2,l/2)$ with $R\subset\mathbb{R}^2$ being the cross-section.

THEOREM 2.4. *Let* $R\subset\mathbb{R}^2$ *be a multiply connected and bounded* C^2 *domain and* $\mathbf{E},\mathbf{H}\in H(\mathrm{curl},G)$ *satisfy the homogeneous Maxwell's equations* (1.2)-(1.3) *and the boundary condition* (1.4) *on* $\partial R\times(-l/2,l/2)$*. If* $k^2\notin\{\lambda_\tau^D\}\cup\{\lambda_\eta^N\}$*, then* $\mathbf{E}$ *and* $\mathbf{H}$ *can be represented as an infinite sum of the following modes converging in* $H(\mathrm{curl},G)$*:*

- *TM modes: for* $\tau=1,\ldots,\infty$*,*

$$\mathbf{E}_\tau^{TM}(\mathbf{x}) = f_\tau^{TM}(x_3)\nabla_2\psi_\tau^D(\mathbf{x}_t) - \frac{\lambda_\tau^D\left(f_\tau^{TM}(x_3)\right)'}{\left(s_\tau^D\right)^2}\psi_\tau^D(\mathbf{x}_t)\mathbf{e}_{x_3}, \tag{2.14}$$

$$\mathbf{H}_\tau^{TM}(\mathbf{x}) = \frac{-\mathbf{i}\omega\epsilon\left(f_\tau^{TM}(x_3)\right)'}{\left(s_\tau^D\right)^2}\mathrm{curl}_2\psi_\tau^D(\mathbf{x}_t), \tag{2.15}$$

$$f_\tau^{TM}(x_3) = d_{\tau,+}^{TM}e^{\mathbf{i}s_\tau^D x_3} + d_{\tau,-}^{TM}e^{-\mathbf{i}s_\tau^D x_3}, \tag{2.16}$$

  where $s_\tau^D=\sqrt{k^2-\lambda_\tau^D}$*, and* $d_{\tau,+}^{TM}, d_{\tau,-}^{TM}$ *are constants.*
- *TE modes: for* $\eta=1,\ldots,\infty$*,*

$$\mathbf{E}_\eta^{TE}(\mathbf{x}) = f_\eta^{TE}(x_3)\mathrm{curl}_2\psi_\eta^N(\mathbf{x}_t), \tag{2.17}$$

$$\mathbf{H}_\eta^{TE}(\mathbf{x}) = \frac{\left(f_\eta^{TE}(x_3)\right)'}{\mathbf{i}\omega\mu_0}\nabla_2\psi_\eta^N(\mathbf{x}_t) + \frac{\lambda_\eta^N f_\eta^{TE}(x_3)}{\mathbf{i}\omega\mu_0}\psi_\eta^N(\mathbf{x}_t)\mathbf{e}_{x_3}, \tag{2.18}$$

$$f_\eta^{TE}(x_3) = d_{\eta,+}^{TE}e^{\mathbf{i}s_\eta^N x_3} + d_{\eta,-}^{TE}e^{-\mathbf{i}s_\eta^N x_3}, \tag{2.19}$$

  where $s_\eta^N=\sqrt{k^2-\lambda_\eta^N}$*, and* $d_{\eta,+}^{TE}, d_{\eta,-}^{TE}$ *are constants.*

- *TEM modes: for* $\zeta = 1, \ldots, N_b$,

$$\mathbf{E}_\zeta^{TEM}(\mathbf{x}) = f_\zeta^{TEM}(x_3)\nabla_2\psi_\zeta^L(\mathbf{x}_t), \tag{2.20}$$

$$\mathbf{H}_\zeta^{TEM}(\mathbf{x}) = -\frac{\left(f_\zeta^{TEM}(x_3)\right)'}{\mathbf{i}\omega\mu}\mathrm{curl}_2\psi_\zeta^L(\mathbf{x}_t), \tag{2.21}$$

$$f_\zeta^{TEM}(x_3) = d_{\zeta,+}^{TEM}e^{\mathbf{i}kx_3} + d_{\zeta,-}^{TEM}e^{-\mathbf{i}kx_3}, \tag{2.22}$$

where $d_{\zeta,+}^{TEM}, d_{\zeta,-}^{TEM}$ *are constants.*

Proof. For each $\mathbf{E} = (E_1, E_2, E_3) \in H(\mathrm{curl}, G)$, let $\mathbf{E}_t := (E_1, E_2)$ and $\mathbf{E}_t^{\mathrm{rot}} := (E_2, -E_1)$. Denote the unit outward normal of $\partial R \times (-l/2, l/2)$ by $\boldsymbol{\nu} = (\nu_1, \nu_2, 0)$. The PEC boundary conditions read as

$$\boldsymbol{\nu} \times \mathbf{E} = (\nu_2 E_3, -\nu_1 E_3, \boldsymbol{\nu} \cdot \mathbf{E}_t^{\mathrm{rot}}) = \mathbf{0}. \tag{2.23}$$

By the Maxwell's equations (1.2)-(1.3), we have

$$H_1 = \frac{\partial_{x_2}E_3 - \partial_{x_3}E_2}{\mathbf{i}\omega\mu_0},\ H_2 = \frac{\partial_{x_3}E_1 - \partial_{x_1}E_3}{\mathbf{i}\omega\mu_0}, \tag{2.24}$$

$$\partial_{x_1}H_3 = \partial_{x_3}H_1 + \mathbf{i}\omega\epsilon E_2,\ \partial_{x_2}H_3 = \partial_{x_3}H_2 - \mathbf{i}\omega\epsilon E_1. \tag{2.25}$$

Substituting H_1 and H_2 from (2.25) into (2.24) leads to

$$\nabla_2 H_3 = \mathbf{i}\omega\epsilon\mathbf{E}_t^{\mathrm{rot}} - \frac{\partial_{x_3}^2\mathbf{E}_t^{\mathrm{rot}}}{\mathbf{i}\omega\mu_0} + \frac{\partial_{x_3}\mathrm{curl}_2 E_3}{\mathbf{i}\omega\mu_0}. \tag{2.26}$$

Additionally, note that $|\boldsymbol{\nu}| = 1$. Thus the conditions $\nu_2 E_3 = \nu_1 E_3 = 0$ give $E_3 = 0$ and that $\boldsymbol{\nu} \cdot \mathrm{curl}_2 E_3 = 0$ on $\partial R \times (-l/2, l/2)$. Furthermore the condition $\boldsymbol{\nu} \cdot \mathbf{E}_t^{\mathrm{rot}} = 0$ results in $\partial_{\boldsymbol{\nu}} H_3 = 0$ on $\partial R \times (-l/2, l/2)$ by using (2.26). Let f_τ^{TM}, f_η^{TE} and f_ζ^{TEM} be the inner product of $\mathbf{E}_t^{\mathrm{rot}}$ with the basis functions over R defined as follows:

$$f_\tau^{TM} := \frac{1}{\lambda_\tau^D}(\mathbf{E}_t^{\mathrm{rot}}(\mathbf{x}), \mathrm{curl}_2\psi_\tau^D(\mathbf{x}_t)), \tag{2.27}$$

$$f_\eta^{TE} := \frac{1}{\lambda_\eta^N}(\mathbf{E}_t^{\mathrm{rot}}(\mathbf{x}), \nabla_2\psi_\eta^N(\mathbf{x}_t)), \tag{2.28}$$

$$f_\zeta^{TEM} := (\mathbf{E}_t^{\mathrm{rot}}(\mathbf{x}), \mathrm{curl}_2\psi_\zeta^L(\mathbf{x}_t)). \tag{2.29}$$

It can be shown that f_τ^{TM}, f_η^{TE}, and f_ζ^{TEM} are governed by ODEs. Taking f_η^{TE} as an example, using the boundary condition $\boldsymbol{\nu} \cdot \mathbf{E}_t^{\mathrm{rot}} = 0$, we have

$$f_\eta^{TE} = -\frac{1}{\lambda_\eta^N}(\mathrm{Curl}\mathbf{E}_t(\mathbf{x}), \psi_\eta^N(\mathbf{x}_t)). \tag{2.30}$$

Then from the Maxwell's equations (1.2)-(1.3), the following equality holds

$$\mathrm{Curl}\mathbf{E}_t = \mathbf{i}\omega\mu_0 H_3 = \frac{\Delta H_3}{\mathbf{i}\omega\epsilon}. \tag{2.31}$$

Substituting $\mathrm{Curl}\mathbf{E}_t$ in (2.30) by (2.31) and applying the Green's formula, we arrive

at

$$
\begin{aligned}
-f_\eta^{TE} =& \frac{1}{\lambda_\eta^N}\left(\frac{\Delta H_3(\mathbf{x})}{\mathbf{i}\omega\epsilon}, \psi_\eta^N(\mathbf{x}_t)\right) \\
=& \frac{1}{\lambda_\eta^N}\left(\frac{\partial_{x_3}^2 H_3(\mathbf{x})}{\mathbf{i}\omega\epsilon}, \psi_\eta^N(\mathbf{x}_t)\right) + \frac{1}{\lambda_\eta^N}\left(\frac{H_3(\mathbf{x})}{\mathbf{i}\omega\epsilon}, \Delta_2\psi_\eta^N(\mathbf{x}_t)\right) \\
=& \frac{1}{k^2}\partial_{x_3}^2 f_\eta^{TE} - \frac{\lambda_\eta^N}{k^2} f_\eta^{TE}. \qquad (2.32)
\end{aligned}
$$

Solving the ODE in (2.32) yields equation (2.19), from which we can construct the corresponding TE mode (2.17)-(2.19) satisfying Maxwell's equations and the PEC boundary condition.

Let $\widetilde{\mathbf{E}}$ and $\widetilde{\mathbf{H}}$ denote the infinite sums

$$
\widetilde{\mathbf{E}} = \sum_\tau^\infty \mathbf{E}_\tau^{TM} + \sum_\eta^\infty \mathbf{E}_\eta^{TE} + \sum_\zeta^{N_b} \mathbf{E}_\zeta^{TEM}, \qquad (2.33)
$$

$$
\widetilde{\mathbf{H}} = \sum_\tau^\infty \mathbf{H}_\tau^{TM} + \sum_\eta^\infty \mathbf{H}_\eta^{TE} + \sum_\zeta^{N_b} \mathbf{H}_\zeta^{TEM}. \qquad (2.34)
$$

If the above sums converge in $H(\mathrm{curl}, G)$, then there holds $\mathbf{E} = \widetilde{\mathbf{E}}$ and $\mathbf{H} = \widetilde{\mathbf{H}}$, since Lemma 2.2 implies $\mathbf{E}_t = \widetilde{\mathbf{E}}_t$ and $\mathbf{H}_t = \widetilde{\mathbf{H}}_t$ for $x_3 \in (-l/2, l/2)$. For ease of presentation, we only show $\sum_\tau^\infty \mathbf{E}_\tau^{TM}$ converge in $[L^2(G)]^3$. Note that

$$
f_\tau^{TM}(x_3) = \frac{1}{\lambda_\tau^D}(\mathbf{E}_t^{\mathrm{rot}}(\mathbf{x}), \mathrm{curl}_2\psi_\tau^D(\mathbf{x}_t)). \qquad (2.35)
$$

Since $\left\{\frac{\nabla_2\psi_\tau^D}{\sqrt{\lambda_\tau^D}}\right\}$ are orthonormal in $[L^2(R)]^2$, a direct computation yields

$$
\sum_\tau^\infty \|f_\tau^{TM}(x_3)\nabla_2\psi_\tau^D(\mathbf{x}_t)\|_{[L^2(G)]^2} \le \|\mathbf{E}_t\|_{[L^2(G)]^2}. \qquad (2.36)
$$

On the other hand, applying the Divergence Theorem and observing that $\mathrm{div}\mathbf{E} = 0$, it can be verified

$$
f_\tau^{TM}(x_3) = \frac{1}{\lambda_\tau^D}\partial_{x_3}(E_3(\mathbf{x}), \psi_\tau^D(\mathbf{x}_t)). \qquad (2.37)
$$

It follows that

$$
(f_\tau^{TM}(x_3))' = \frac{1}{\lambda_\tau^D}\partial_{x_3}^2(E_3(\mathbf{x}), \psi_\tau^D(\mathbf{x}_t)) = -\frac{(s_\tau^D)^2}{\lambda_\tau^D}(E_3(\mathbf{x}), \psi_\tau^D(\mathbf{x}_t)). \qquad (2.38)
$$

Therefore, from the orthonormal properties of $\{\psi_\tau^D\}$ in $L^2(R)$ (cf. Theorem 4.12 in [35]), we have

$$
\sum_\tau^\infty \left\| \frac{\lambda_\tau^D \left(f_\tau^{TM}(x_3)\right)'}{\left(s_\tau^D\right)^2}\psi_\tau^D(\mathbf{x}_t) \right\|_{L^2(G)} \le \|E_3\|_{L^2(G)}. \qquad (2.39)
$$

∎

2.5. The single-layer potential. We introduce the single-layer potential $\mathcal{K}_0$ on $(0,1)$:

$$(\mathcal{K}_0[\phi])(r) := 2\int_0^1 \frac{1}{2\pi}\log\frac{1}{|r-r'|}\phi(r')ds(r'), \tag{2.40}$$

and an orthogonal basis:

$$\phi_n(r) = \begin{cases} \dfrac{1}{\sqrt{2}}\cos(n\pi r), & n\in\mathbb{N}^*; \\ 1, & n=0. \end{cases} \tag{2.41}$$

Equivalent norms of $H^{1/2}((0,1))$ and $\widetilde{H}^{-1/2}((0,1))$ can be defined as

$$\|f\|^2_{H^{1/2}(0,1)} := \sum_{n=0}^{\infty}(1+n^2)^{1/2}|(f,\phi_n)|^2,$$

$$\|f\|^2_{\widetilde{H}^{-1/2}(0,1)} := \sum_{n=0}^{\infty}(1+n^2)^{-1/2}|(f,\phi_n)|^2.$$

3. Analysis of the resonances. In this section, we analyze the resonances for the scattering problem (1.2) - (1.5). We first decompose the electromagnetic fields into even and odd functions using the reflection symmetry of the problem geometry. We then introduce the Tangential-to-Tangential (T2T) map on the hole apertures to reduce Maxwell's equations above the metal to boundary integral equations over the hole apertures. By expanding the electromagnetic field within annular holes as a sum of TM, TE, and TEM modes and matching the electromagnetic field over the hole apertures, we set up an equivalent infinite-dimensional linear system for the mode expansion coefficients. This leads to a nonlinear characteristic equation (resonance condition) when the solution of the infinite linear system is projected onto a dominant mode whose perturbation yields a resonance. Finally we perform the asymptotic analysis of resonances when $h \ll 1$ from the resonant condition and analyze near-field enhancement at resonant frequencies.

3.1. Decomposition of the scattering problem. Due to the reflection symmetry of our structure to the x_1x_2 plane, if the pair $(\mathbf{E}(\mathbf{x}),\mathbf{H}(\mathbf{x}))$ satisfies the Maxwell system (1.2)-(1.4), so does $(\mathbf{E}^*(\mathbf{x}^*),-\mathbf{H}^*(\mathbf{x}^*))$. Therefore, we can define the even and odd solutions to the scattering problem by

$$(\mathbf{E}^{(e)}(\mathbf{x}),\mathbf{H}^{(e)}(\mathbf{x})) = (\mathbf{E}(\mathbf{x}),\mathbf{H}(\mathbf{x})) + (\mathbf{E}^*(\mathbf{x}^*),-\mathbf{H}^*(\mathbf{x}^*)); \tag{3.1}$$

$$(\mathbf{E}^{(o)}(\mathbf{x}),\mathbf{H}^{(o)}(\mathbf{x})) = (\mathbf{E}(\mathbf{x}),\mathbf{H}(\mathbf{x})) - (\mathbf{E}^*(\mathbf{x}^*),-\mathbf{H}^*(\mathbf{x}^*)), \tag{3.2}$$

which satisfies the boundary conditions $\gamma_T(\mathbf{H}^{(e)})=0$ or $\gamma_t(\mathbf{E}^{(o)})=0$ on the interface $R^h\times\{x_3=0\}$ respectively. Accordingly, the scattering problem can be decomposed into an even scattering problem and an odd scattering problem that are both defined in a domain in the upper half-space $\mathbb{R}^3_+$. In what follows, we focus only on the even scattering problem with the boundary condition $\gamma_T(\mathbf{H}^{(e)})=0$. The analysis for the odd scattering problem is similar. For ease of notation, we suppress the superscript (e) in the sequel.

3.2. The T2T map on the aperture. Similar to the NtD and DtN maps for the Helmholtz equation, the tangential-to-tangential (T2T) map enables us to reduce the 3D Maxwell's equations into integral equations defined on the boundary.

For vector field $\mathbf{F} = (F_1, F_2, 0)^T$ on A^h, we define the following vector layer potentials

$$\mathcal{M}_k[\mathbf{F}](\mathbf{x}) := \mathrm{curl} \int_{A^h} \Phi_k(\mathbf{x};\mathbf{x}')\mathbf{F}(\mathbf{x}')d\mathbf{x}', \tag{3.3}$$

$$\mathcal{L}_k[\mathbf{F}](\mathbf{x}) := \mathrm{curlcurl} \int_{A^h} \Phi_k(\mathbf{x};\mathbf{x}')\mathbf{F}(\mathbf{x}')d\mathbf{x}', \tag{3.4}$$

where $\Phi_k(\mathbf{x},\mathbf{x}') := \frac{e^{\mathbf{i}k|\mathbf{x}-\mathbf{x}'|}}{4\pi|\mathbf{x}-\mathbf{x}'|}$. The following theorem introduces the T2T map.

THEOREM 3.1. *Assume $k \in \mathbb{R}_+$. For any $\mathbf{E}$, $\mathbf{H} \in H_{\mathrm{loc}}(\mathrm{curl}, \mathbb{R}^3_+)$ satisfying the Maxwell's equations* (1.2)-(1.4) *and the Silver-Müller radiation condition* (1.5) *above the metal, we have*

$$\mathbf{E}(\mathbf{x}) = -2\mathcal{M}_k[\gamma_t(\mathbf{E})](\mathbf{x}),\ \mathbf{H}(\mathbf{x}) = -\frac{2}{\mathbf{i}\omega\mu_0}\mathcal{L}_k[\gamma_t(\mathbf{E})](\mathbf{x}). \tag{3.5}$$

Moreover, the T2T map $\gamma_T \circ \mathcal{L}_k$ is bounded from $\widetilde{H}^{-1/2}(\mathrm{Div}, A^h)$ to $H^{-1/2}(\mathrm{Curl}, A^h)$.

Proof. Assuming $\mathbf{F} \in \widetilde{H}^{-1/2}(\mathrm{Div}, A^h)$, it can be verified that the potentials $-2\mathcal{M}_k[\mathbf{F}]$ and $-\frac{2}{\mathbf{i}\omega\mu_0}\mathcal{L}_k[\mathbf{F}]$ satisfy the Maxwell's equations (1.2)-(1.4) and the radiation condition (1.5). Moreover, using the jump relations of single layer potential defined by Φ_k on $\mathbb{R}^3_+$, the identity $\mathbf{F} = -2\gamma_t \circ \mathcal{M}_k[\mathbf{F}]$ holds. Hence the equation (3.5) follows from the uniqueness of the scattering problem.

To prove the boundedness of $\gamma_T \circ \mathcal{L}_k$, it's enough to show $\mathcal{M}_k$ is bounded from $\widetilde{H}^{-1/2}(\mathrm{Div}, A^h)$ to $H_{\mathrm{loc}}(\mathrm{curl}, \mathbb{R}^3_+)$, which is a consequence of the properties of single layer potential defined by Φ_k (cf. Theorem 6.11 in [35]). ∎

We introduce the trace of the single-layer potential $\mathcal{S}_k : \widetilde{H}^{-1/2}(A^h) \to H^{1/2}(A^h)$:

$$\mathcal{S}_k[\phi](\mathbf{x}) := \int_{A^h} \Phi_k(\mathbf{x},\mathbf{x}')\phi(\mathbf{x}')dS(\mathbf{x}'). \tag{3.6}$$

The sesquilinear form induced by $\gamma_T \circ \mathcal{L}_k$ has the following properties.

LEMMA 3.2 (Lemma 5.61 in [23]). *For any $\mathbf{F}, \mathbf{G} \in \widetilde{H}^{-1/2}(\mathrm{Div}, A^h)$,*

$$(\gamma_T \circ \mathcal{L}_k[\mathbf{F}], \mathbf{G}) = (\gamma_T \circ \mathcal{L}_k[\overline{\mathbf{G}}], \overline{\mathbf{F}}), \tag{3.7}$$

$$(\gamma_T \circ \mathcal{L}_k[\mathbf{F}], \mathbf{G}) = -(\mathcal{S}_k[\mathrm{Div}\mathbf{F}], \mathrm{Div}\mathbf{G}) + k^2(\mathcal{S}_k[\mathbf{F}], \mathbf{G}). \tag{3.8}$$

3.3. Field expansion in annular holes. According to Theorem 2.4, the electromagnetic field in each annular hole $G^{h_p}_{+,p}$, $p = 1, \ldots, P$, can be expanded by the sum of TM, TE, and TEM modes as (2.14)-(2.22). Exploiting the simple geometry of annular holes, the Dirichlet and Neumann eigenpairs over the cross-sectional annulus

$R_p^{h_p}$ can be expressed explicitly as follows:

$$\lambda_{i,j,p}^D = (\beta_{|i|,j,p}^D)^2, \tag{3.9}$$

$$\begin{aligned}\psi_{i,j,p}^D(r,\theta) = &\left(C_{i,j,p}^D\right)^{-1}\left[Y_{|i|}(\beta_{|i|,j,p}^D a_p)J_{|i|}(\beta_{|i|,j,p}^D r)\right.\\ &\left. - J_{|i|}(\beta_{|i|,j,p}^D a_p)Y_{|i|}(\beta_{|i|,j,p}^D r)\right]e^{\mathbf{i}i\theta},\end{aligned} \tag{3.10}$$

$$\lambda_{m,n,p}^N = (\beta_{|m|,n,p}^N)^2, \tag{3.11}$$

$$\begin{aligned}\psi_{m,n,p}^N(r,\theta) = &\left(C_{m,n,p}^N\right)^{-1}\left[Y'_{|m|}(\beta_{|m|,n,p}^N a_p)J_{|m|}(\beta_{|m|,n,p}^N r)\right.\\ &\left. - J'_{|m|}(\beta_{|m|,n,p}^N a_p)Y_{|m|}(\beta_{|m|,n,p}^N r)\right]e^{\mathbf{i}m\theta}.\end{aligned} \tag{3.12}$$

Here, $(i,j) \in \mathbb{Z}\times\mathbb{N}^*$,$(m,n) \in (\mathbb{Z}\times\mathbb{N})^*$, $Y_{|i|}(\cdot)$ and $J_{|i|}(\cdot)$ are Bessel functions, and $\beta_{|i|,j,p}^D$ and $\beta_{|m|,n,p}^N$ denote the j-th and n-th roots of the following functions respectively

$$F_{i,p}^D(\beta) = Y_{|i|}(\beta a_p)J_{|i|}(\beta a_p(1+h_p)) - J_{|i|}(\beta a_p)Y_{|i|}(\beta a_p(1+h_p)), \tag{3.13}$$

$$F_{m,p}^N(\beta) = Y'_{|m|}(\beta a_p)J'_{|m|}(\beta a_p(1+h_p)) - J'_{|m|}(\beta a_p)Y'_{|m|}(\beta a_p(1+h_p)). \tag{3.14}$$

Additionally, $\psi_p^L = \log r/\sqrt{2\pi\log(1+h_p)}$.

In the sequel, we refer to the index i in the eigen-pair $(\lambda_{i,j,p}^D, \psi_{i,j,p}^D)$ as the angular momentum, since $\psi_{i,j,p}^D$ depends on the angular variable θ in the form $e^{im\theta}$. Similarly, we refer to the index m in the eigen-pair $(\lambda_{m,n,p}^N, \psi_{m,n,p}^N)$ as the angular momentum.

Using the boundary condition $\gamma_T(\mathbf{H}) = 0$ on $R^h \times \{x_3 = 0\}$, it follows that $d_{i,j,p,+}^{TM} = d_{i,j,p,-}^{TM}$, $d_{m,n,p,+}^{TE} = d_{m,n,p,-}^{TE}$, and $d_{p,+}^{TEM} = d_{p,-}^{TEM}$, hence the following expansions hold:

$$\mathbf{E} = \sum_{(i,j)\in\mathbb{Z}\times\mathbb{N}^*} d_{i,j,p}^{TM}\mathbf{E}_{i,j,p}^{TM} + \sum_{(m,n)\in(\mathbb{Z}\times\mathbb{N})^*} d_{m,n,p}^{TE}\mathbf{E}_{m,n,p}^{TE} + d_p^{TEM}\mathbf{E}_p^{TEM}, \tag{3.15}$$

$$\mathbf{H} = \sum_{(i,j)\in\mathbb{Z}\times\mathbb{N}^*} d_{i,j,p}^{TM}\mathbf{H}_{i,j,p}^{TM} + \sum_{(m,n)\in(\mathbb{Z}\times\mathbb{N})^*} d_{m,n,p}^{TE}\mathbf{H}_{m,n,p}^{TE} + d_p^{TEM}\mathbf{H}_p^{TEM}. \tag{3.16}$$

Then the continuity of trace maps leads to the following expansions on each aperture $A_p^{h_p}$ $(p = 1,\dots,P)$:

$$\begin{aligned}\gamma_t(\mathbf{E})\mathcal{X}_p\big|_{A_p^{h_p}} = &\sum_{(i,j)\in\mathbb{Z}\times\mathbb{N}^*} d_{i,j,p}^{TM} 2\cos(s_{i,j,p}^D l/2)\mathrm{curl}_2\psi_{i,j,p}^D\\ &- \sum_{(m,n)\in(\mathbb{Z}\times\mathbb{N})^*} d_{m,n,p}^{TE} 2\cos(s_{m,n,p}^N l/2)\nabla_2\psi_{m,n,p}^N\\ &+ d_p^{TEM} 2\cos(\sqrt{\epsilon_r}kl/2)\mathrm{curl}_2\log r\mathcal{X}_p,\end{aligned} \tag{3.17}$$

$$\begin{aligned}\gamma_T(\mathbf{H})\mathcal{X}_p\big|_{A_p^{h_p}} = &\sum_{(i,j)\in\mathbb{Z}\times\mathbb{N}^*} \frac{d_{i,j,p}^{TM} 2\mathbf{i}\omega\epsilon_1\sin(s_{i,j,p}^D l/2)}{s_{i,j,p}^D}\mathrm{curl}_2\psi_{i,j,p}^D\\ &+ \sum_{(m,n)\in(\mathbb{Z}\times\mathbb{N})^*} \frac{d_{m,n,p}^{TE} 2\mathbf{i}s_{m,n,p}^N\sin(s_{m,n,p}^N l/2)}{\omega\mu_0}\nabla_2\psi_{m,n,p}^N\\ &+ d_p^{TEM}\frac{2\sqrt{\epsilon_1}\sin(\sqrt{\epsilon_r}kl/2)}{\mathbf{i}\sqrt{\mu_0}}\mathrm{curl}_2\log r\mathcal{X}_p,\end{aligned} \tag{3.18}$$

where $\epsilon_r := \epsilon_1/\epsilon_0$ is the relative electric permittivity. Note that the wavenumber in each annular hole is $\sqrt{\epsilon_r}k$.

In what follows, we use the negative imaginary axis as the branch cut of $\sqrt{\cdot}$ in the definitions of $s^D_{i,j,p}$ and $s^N_{m,n,p}$ to ensure the analyticity when k attains a minor negative imaginary part.

3.4. Equivalent infinite linear system. In light of Lemma 2.2, we observe the set $\{\mathrm{curl}_2\psi^D_{i,j,p}, \nabla_2\psi^N_{m,n,p}, \nabla_2\psi^L_p\}$ forms an orthogonal basis for $\widetilde{H}^{-1/2}(\mathrm{Div}, R^{h_p}_p)$ and $H^{-1/2}(\mathrm{Curl}, R^{h_p}_p)$. The T2T map $\gamma_T\circ\mathcal{L}_k$ can be represented by an infinite-dimensional matrix under this basis, which maps the coefficients of the expansion (3.17) to that of the expansion (3.18). Furthermore, taking advantage of the rotation symmetry of the annulus structure, the infinite-dimensional linear system can be decoupled into a sequence of infinite-dimensional subsystems according to the angular momentum of the eigenbasis. This is because the interactions between the eigenbasis with different angular momentum vanish in the sense that

$$(\gamma_T \circ \mathcal{L}_k\nabla_2\psi^N_{m,n,p}, \nabla_2\psi^N_{m',n',p'}) = 0, \text{ if } m \neq m', \tag{3.19}$$

$$(\gamma_T \circ \mathcal{L}_k\nabla_2\psi^N_{m,n,p}, \mathrm{curl}_2\psi^D_{i',j',p'}) = 0, \text{ if } m \neq i', \tag{3.20}$$

$$(\gamma_T \circ \mathcal{L}_k\nabla_2\psi^N_{m,n,p}, \mathrm{curl}_2\log r\mathcal{X}_{p'}) = 0, \text{ if } m \neq 0, \tag{3.21}$$

$$(\gamma_T \circ \mathcal{L}_k\mathrm{curl}_2\psi^D_{i,j,p}, \mathrm{curl}_2\psi^D_{i',j',p'}) = 0, \text{ if } i \neq i', \tag{3.22}$$

$$(\gamma_T \circ \mathcal{L}_k\mathrm{curl}_2\psi^D_{i,j,p}, \mathrm{curl}_2\log r\mathcal{X}_{p'}) = 0, \text{ if } i \neq 0, \tag{3.23}$$

where (m,n), $(m',n') \in (\mathbb{Z}\times\mathbb{N})^*$, (i,j), $(i',j') \in \mathbb{Z}\times\mathbb{N}^*$ and $p,p' = 1,\ldots,P$ (cf. Lemma 4.2 in [28]).

We now focus on a subsystem with angular momentum $m = m' = i = i' \neq 0$. It takes the following specific forms for $p,p' = 1,\ldots,P$

$$D_{m,p'}d^{TE}_{m,0,p'} - \sum_{p=1}^{P} A_{m,p',p}d^{TE}_{m,0,p} - \sum_{p=1}^{P}\mathbf{R}^{TE}_{m,p',p}\mathbf{c}^{TE}_{m,p} - \sum_{p=1}^{P}\mathbf{R}^{TM}_{m,p',p}\mathbf{c}^{TM}_{m,p} = 0, \tag{3.24}$$

$$\mathbf{c}^{TE}_{m,p'} - \sum_{p=1}^{P}\mathbf{C}^{TE}_{m,p',p}d^{TE}_{m,0,p} - \sum_{p=1}^{P}\mathbf{B}^{TE,TE}_{m,p',p}\mathbf{c}^{TE}_{m,p} - \sum_{p=1}^{P}\mathbf{B}^{TE,TM}_{m,p',p}\mathbf{c}^{TM}_{m,p} = \mathbf{0}, \tag{3.25}$$

$$\mathbf{c}^{TM}_{m,p'} - \sum_{p=1}^{P}\mathbf{C}^{TM}_{m,p',p}d^{TE}_{m,0,p} - \sum_{p=1}^{P}\mathbf{B}^{TM,TE}_{m,p',p}\mathbf{c}^{TE}_{m,p} - \sum_{p=1}^{P}\mathbf{B}^{TM,TM}_{m,p',p}\mathbf{c}^{TM}_{m,p} = \mathbf{0}, \tag{3.26}$$

where $\mathbf{c}^{TE}_{m,p}$ and $\mathbf{c}^{TM}_{m,p}$ are rescaled Fourier coefficients:

$$\mathbf{c}^{TE}_{m,p'} = \Big[(\lambda_{m,n',p'})^{3/4}\sin(s^N_{m,n',p'}l/2)d^{TE}_{m,n',p'}\Big]_{n'\in\mathbb{N}^*}, \tag{3.27}$$

$$\mathbf{c}^{TM}_{m,p'} = \Big[(\lambda_{m,j',p'})^{1/4}\sin(s^D_{m,j',p'}l/2)d^{TM}_{m,j',p'}\Big]_{j'\in\mathbb{N}^*}. \tag{3.28}$$

Additionally, $D_{m,p'}$ and $A_{m,p',p}$ are scalars, $\mathbf{C}^{TE}_{m,p',p}$, $\mathbf{C}^{TM}_{m,p',p}$, are infinite-dimensional column vectors, while $\mathbf{R}^{TE}_{m,p',p}$ and $\mathbf{R}^{TM}_{m,p',p}$ are infinite-dimensional row vectors, and $\mathbf{B}^{TE,TE}_{m,p',p}$, $\mathbf{B}^{TE,TM}_{m,p',p}$, $\mathbf{B}^{TM,TE}_{m,p',p}$, $\mathbf{B}^{TM,TM}_{m,p',p}$ are regarded as matrices of infinite dimension.

More specifically, we have the following expressions:

$$
\begin{aligned}
D_{m,p'} =& s^N_{m,0,p'} \sin(s^N_{m,0,p'} l/2),\\
A_{m,p',p} =& -2\cos(s^N_{m,0,p} l/2)(\lambda^N_{m,0,p'})^{-1}(\gamma_T \circ \mathcal{L}_k \nabla_2 \psi^N_{m,0,p}, \nabla_2 \psi^N_{m,0,p'}),\\
\mathbf{R}^{TE}_{m,p',p} =& \left[\frac{-2\cot(s^N_{m,n,p} l/2)(\gamma_T \circ \mathcal{L}_k \nabla_2 \psi^N_{m,n,p}, \nabla_2 \psi^N_{m,0,p'})}{\lambda^N_{m,0,p'}(\lambda^N_{m,n,p})^{3/4}}\right]_{n\in\mathbb{N}^*},\\
\mathbf{R}^{TM}_{m,p',p} =& \left[\frac{-2\cot(s^D_{m,j,p} l/2)(\gamma_T \circ \mathcal{L}_k \mathrm{curl}_2 \psi^D_{m,j,p}, \nabla_2 \psi^N_{m,0,p'})}{\lambda^N_{m,0,p'}(\lambda^D_{m,j,p})^{1/4}}\right]_{j\in\mathbb{N}^*},\\
\mathbf{C}^{TE}_{m,p',p} =& \left[\frac{-2\cos(s^N_{m,0,p} l/2)(\gamma_T \circ \mathcal{L}_k \nabla_2 \psi^N_{m,0,p}, \nabla_2 \psi^N_{m,n',p'})}{(\lambda^N_{m,n',p'})^{1/4} s^N_{m,n',p'}}\right]_{n'\in\mathbb{N}^*},\\
\mathbf{C}^{TM}_{m,p',p} =& \left[\frac{-2s^D_{m,j',p'}\cos(s^N_{m,0,p} l/2)(\gamma_T \circ \mathcal{L}_k \nabla_2 \psi^N_{m,0,p}, \mathrm{curl}_2 \psi^D_{m,j',p'})}{\epsilon_r k^2 (\lambda^D_{m,j',p'})^{3/4}}\right]_{j'\in\mathbb{N}^*},\\
\mathbf{B}^{TE,TE}_{m,p',p} =& \left[\frac{-2\cot(s^N_{m,n,p} l/2)(\gamma_T \circ \mathcal{L}_k \nabla_2 \psi^N_{m,n,p}, \nabla_2 \psi^N_{m,n',p'})}{(\lambda^N_{m,n',p'})^{1/4}(\lambda^N_{m,n,p})^{3/4} s^N_{m,n,p}}\right]_{n',n\in\mathbb{N}^*},\\
\mathbf{B}^{TM,TE}_{m,p',p} =& \left[\frac{-2s^D_{m,j',p'}\cot(s^N_{m,n,p} l/2)(\gamma_T \circ \mathcal{L}_k \nabla_2 \psi^N_{m,n,p}, \mathrm{curl}_2 \psi^D_{m,j',p'})}{\epsilon_r k^2 (\lambda^D_{m,j',p'})^{3/4}(\lambda^N_{m,n,p})^{3/4}}\right]_{j',n\in\mathbb{N}^*},\\
\mathbf{B}^{TE,TM}_{m,p',p} =& \left[\frac{-2\cot(s^D_{m,j,p} l/2)(\gamma_T \circ \mathcal{L}_k \mathrm{curl}_2 \psi^D_{m,j,p}, \nabla_2 \psi^N_{m,n',p'})}{(\lambda^N_{m,n',p'})^{1/4}(\lambda^D_{m,j,p})^{1/4} s^N_{m,n',p'}}\right]_{n',j\in\mathbb{N}^*},\\
\mathbf{B}^{TM,TM}_{m,p',p} =& \left[\frac{-2s^D_{m,j',p'}\cot(s^D_{m,j,p} l/2)(\gamma_T \circ \mathcal{L}_k \mathrm{curl}_2 \psi^D_{m,j,p}, \mathrm{curl}_2 \psi^D_{m,j',p'})}{\epsilon_r k^2 (\lambda^D_{m,j',p'})^{3/4}(\lambda^D_{m,j,p})^{1/4}}\right]_{j',j\in\mathbb{N}^*}.
\end{aligned}
$$

Here the row indices are denoted by $n', j' \in \mathbb{N}^*$ and the column indices are denoted by $n, j \in \mathbb{N}^*$.

3.5. Resonance condition. In this subsection, we derive the resonance condition for the subsystems with nonzero angular momentum. We remark that the leading order of resonances with zero-angular-momentum is independent of the radii of the annular gaps.

We first introduce the matrix $\mathbf{U} := (u_{n',n})_{n',n\in\mathbb{N}^*}$ and vector $\mathbf{u} := (u_{n',0})_{n'\in\mathbb{N}^*}$ where

$$
u_{n',n} := \begin{cases} (\mathcal{K}_0[(n'\pi)^{1/2}\phi_{n'}], (n\pi)^{1/2}\phi_n), & \text{if } n, n' \in \mathbb{N}^*;\\ (\mathcal{K}_0[(n'\pi)^{1/2}\phi_{n'}], \phi_0), & \text{if } n = 0, n' \in \mathbb{N}^*. \end{cases}
$$

Here ϕ_n's are defined in (2.41). The following lemma plays a key role in reducing our linear system (3.24)-(3.26) to finite dimensions.

LEMMA 3.3. *Let* $\mathbf{I}$ *be the identity operator on* ℓ^2*. For any* $b > 0$, $b\mathbf{I}+\mathbf{U}$ *is bounded and invertible from* ℓ^2 *to* ℓ^2*.*

Proof. From the Theorem 8.12 in [35], we know $\mathbf{U}$ is bounded and for any $\mathbf{v} \in \ell^2$

$$
(\mathbf{U}\mathbf{v}, \mathbf{v}) > 0,
$$

which implies $b\mathbf{I}+\mathbf{U}$ is positive and bounded below. Then the invertibility of the operator $b\mathbf{I}+\mathbf{U}$ follows from the Lax-Milgram theorem. ∎

For $p,p'=1,\ldots,P$, we denote

$$\begin{aligned}
\mathbf{A}_m :=&(A_{m,p,p'})_{p,p'=1}^{P},\\
\mathbf{B}_m :=&(\mathbf{B}_{m,p,p'})_{p,p'=1}^{P},\ \text{where } \mathbf{B}_{m,p,p'} := \begin{bmatrix} \mathbf{B}_{m,p,p'}^{TE,TE} & \mathbf{B}_{m,p,p'}^{TE,TM} \\ \mathbf{B}_{m,p,p'}^{TM,TE} & \mathbf{B}_{m,p,p'}^{TM,TM} \end{bmatrix},\\
\mathbf{C}_m :=&(\mathbf{C}_{m,p,p'})_{p,p'=1}^{P},\ \text{where } \mathbf{C}_{m,p,p'} := \begin{bmatrix} \mathbf{C}_{m,p,p'}^{TE} \\ \mathbf{C}_{m,p,p'}^{TM} \end{bmatrix},\\
\mathbf{R}_m :=&(\mathbf{R}_{m,p,p'})_{p,p'=1}^{P},\ \text{where } \mathbf{R}_{m,p,p'} := \begin{bmatrix} \mathbf{R}_{m,p,p'}^{TE} & \mathbf{R}_{m,p,p'}^{TM} \end{bmatrix},\\
\mathbf{D}_m :=&\mathrm{Diag}\{(D_{m,p})_{p=1}^{P}\},\\
\mathbf{d}_m :=&(d_{m,0,p}^{TE})_{p=1}^{P},\ \text{and}\\
\mathbf{I}_{2P} :=&\mathrm{Diag}\{(\mathbf{I})_{p=1}^{2P}\}.
\end{aligned}$$

Thanks to the asymptotic expansions derived in [28] for each matrix and vector element in the subsystem (3.24)-(3.26) for $p=p'$, we can follow the same lines to derive the leading-order dependence of the elements to h for $p\neq p'$. Lemma 3.3 implies the invertibility of $\mathbf{I}_{2P}-\mathbf{B}_m$ for $h\ll 1$ (See [28] for detail), as such the system (3.24)-(3.26) can be reduced to

$$\left[\mathbf{D}_m(k)-\mathbf{A}_m(k)-\mathbf{R}_m(k)\left(\mathbf{I}_{2P}-\mathbf{B}_m(k)\right)^{-1}\mathbf{C}_m(k)\right]\mathbf{d}_m=\mathbf{0}, \tag{3.29}$$

where the dependence on k is made explicit. We call (3.29) the characteristic equation, which yields the resonance condition for the scattering problem.

Remark 3.4. (3.29) gives the resonance condition for the scattering problem with even resonant modes, wherein the boundary condition $\gamma_T(\mathbf{H})=0$ is enforced on the interface $R^h\times\{x_3=0\}$. Following the parallel derivation, the resonance condition for the scattering problem with the odd resonant modes can be set up by replacing $\sin(\cdot)$ in $\mathbf{D}_m$ by $\cos(\cdot)$, and $\cos(\cdot)$ in $\mathbf{A}_m$, $\mathbf{R}_m$, $\mathbf{B}_m$, and $\mathbf{C}_m$ by $-\sin(\cdot)$.

3.6. Asymptotic analysis of resonances. We introduce the following auxiliary functions for $p,p'=1,\ldots,P$, $p\neq p'$:

$$\begin{aligned}
\Pi_{m,p,p}(x) =&\left[\frac{m^2}{a_p\pi}\left(\alpha_m(a_px)+\mathbf{i}\beta_m(a_px)\right)-\frac{x^2a_p}{\pi}\left(\widetilde{\alpha}_m(a_px)+\mathbf{i}\widetilde{\beta}_m(a_px)\right)\right.\\
&\left.-4\frac{m^2}{a_p}\mathbf{u}^T\left(\mathbf{I}+4\mathbf{U}\right)^{-1}\mathbf{u}+4x^2a_p\mathbf{u}^T\left(\epsilon_r\mathbf{I}+4\mathbf{U}\right)^{-1}\mathbf{u}\right]h_p,\\
\Pi_{m,p,p'}(x) =&\mathcal{O}(h),
\end{aligned}$$

where

$$\alpha_m(x) := \int_0^{\pi/2} \frac{\cos(2x\sin(\theta)) - 1}{\sin(\theta)} \cos(2m\theta) d\theta + \frac{3}{2} + \log 2 - \gamma - \psi(|m| + 1/2),$$

$$\beta_m(x) := \int_0^{\pi/2} \frac{\sin(2x\sin(\theta))}{\sin(\theta)} \cos(2m\theta) d\theta,$$

$$\widetilde{\alpha}_m(x) := \frac{\alpha_{m-1}(x) + \alpha_{m+1}(x)}{2},$$

$$\widetilde{\beta}_m(x) := \frac{\beta_{m-1}(x) + \beta_{m+1}(x)}{2},$$

γ is the Euler constant and $\psi(\cdot)$ denotes the digamma function. The following theorem gives the asymptotic expansions of resonances.

THEOREM 3.5. *Assuming $h_p \le h \ll 1$, $p = 1, \dots, P$, for $m \in \mathbb{Z}^*$ and $m' \in \mathbb{N}$, there exist resonances*

$$k_{m,m',p} = k^{(1)}_{m,m',p} + \mathcal{O}(h \log h), \text{ where } k^{(1)}_{m,m',p} = \frac{1}{\sqrt{\epsilon_r}} \sqrt{\left(\frac{m}{a_p}\right)^2 + \left(\frac{m'\pi}{l}\right)^2}. \tag{3.30}$$

Moreover, for a given resonance $k_{m,m',p}$, if

$$k^{(1)}_{m,m',p} \neq k^{(1)}_{m,m'',p'}, \tag{3.31}$$

holds for $p \neq p'$, $m'' = m' \bmod 2$, then the following asymptotic expansions hold:

$$\begin{aligned} k_{m,0,p} =& k^{(1)}_{m,0,p} - \left(\frac{m^2}{a_p^2} - (k^{(1)}_{m,0,p})^2\right) \frac{a_p}{\pi l \epsilon_r k^{(1)}_{m,0,p}} h_p \log h_p - \frac{m^2}{2a_p^2 \epsilon_r k^{(1)}_{m,0,p}} h_p \\ &+ \frac{1}{l\epsilon_r k^{(1)}_{m,0,p}} \Pi_{m,p,p}\left(k^{(1)}_{m,0,p}\right) + O(h^2 \log^2 h), \end{aligned} \tag{3.32}$$

$$\begin{aligned} k_{m,m',p} =& k^{(1)}_{m,m',p} - \left(\frac{m^2}{a_p^2} - (k^{(1)}_{m,m',p})^2\right) \frac{2a_p}{\pi l \epsilon_r k^{(1)}_{m,m',p}} h_p \log h_p - \frac{m^2}{2a_p^2 \epsilon_r k^{(1)}_{m,m',p}} h_p \\ &+ \frac{2}{l\epsilon_r k^{(1)}_{m,m',p}} \Pi_{m,p,p}\left(k^{(1)}_{m,m',p}\right) + O(h^2 \log^2 h), \quad (m' \neq 0). \end{aligned} \tag{3.33}$$

Proof. For clarity, we prove for $P = 2$ and consider (3.29) for the even resonant modes. The proof for $P > 2$ and the odd resonant modes is similar. By expanding each term in the system (3.29), we have

$$\begin{aligned} \mathbf{D}(k) :=& \mathrm{Diag}\left\{ \left(s^N_{m,0,p} \tan(s^N_{m,0,p} l/2) - \left(\frac{m^2}{a_p^2} - k^2\right) \frac{a_p}{\pi} h_p \log h_p - \Pi_{m,p,p}(k) \right)^2_{p=1} \right\} \\ &- \begin{bmatrix} 0 & \Pi_{m,1,2}(k) \\ \Pi_{m,2,1}(k) & 0 \end{bmatrix} + \mathcal{O}(h^2 \log h), \end{aligned} \tag{3.34}$$

which is rank-deficient if k is a resonance. A direct computations of $\det(\mathbf{D}(k))$ yields

$$\det(\mathbf{D}(k)) = \left(s^N_{m,0,1}\tan(s^N_{m,0,1}l/2) - \left(\frac{m^2}{a_1^2} - k^2\right)\frac{a_1}{\pi}h_1\log h_1 - \Pi_{m,1,1}(k)\right)\cdot$$
$$\left(s^N_{m,0,2}\tan(s^N_{m,0,2}l/2) - \left(\frac{m^2}{a_2^2} - k^2\right)\frac{a_2}{\pi}h_2\log h_2 - \Pi_{m,2,2}(k)\right)$$
$$+\mathcal{O}(h^2\log h), \tag{3.35}$$

where $\Pi_{m,p,p}(k) = \mathcal{O}(h)$, $p = 1, 2$. Solving (3.34) above gives the expansion (3.30). We then take the ansatz $k = k^{(1)}_{m,m',1} + k^{(2)}$, $k^{(2)} = o(1)$, in (3.35). If (3.31) holds, then $s^N_{m,0,2}\tan(s^N_{m,0,2}l/2) = \mathcal{O}(1)$, and we obtain the expansions (3.32)-(3.33) by noting that

$$s^N_{m,0,1}\tan(s^N_{m,0,1}l/2) = \left(2k^{(1)}_{m,m',1}k^{(2)} + \frac{m^2}{a_1^2}h_1\right)\frac{l}{4-2\delta_{m',0}} + \mathcal{O}((k^{(2)})^2), \tag{3.36}$$

where $\delta_{m',0}$ denotes Kronecker delta function.

We next show the existence of resonances by Brouwer's fixed-point theorem. Letting $|k^{(2)}| \le \sqrt{h}$ in the ansatz, then there exists $c \in \mathbb{C}$ and $c \neq 0$ such that

$$k^{(2)} - c\cdot\det(\mathbf{D}(k^{(1)}_{m,m',1} + k^{(2)})) = \mathcal{O}(h\log h). \tag{3.37}$$

Note that the term $s^N_{m,0,p}\tan(s^N_{m,0,p}l/2)$ is analytic even if $\sqrt{\epsilon_r k^2 - \lambda^N_{m,0,1}}$ tends to zero. The continuity of (3.37) implies the existence of resonance. ∎

3.7. Field enhancement at resonant frequencies. Consider an incident field illuminating the metal from below with the form

$$\mathbf{E}^{\text{inc}} = \begin{bmatrix}0\\1\\0\end{bmatrix}e^{\mathbf{i}k\mathbf{x}\cdot\mathbf{d}}, \mathbf{H}^{\text{inc}} = \sqrt{\frac{\epsilon_0}{\mu_0}}\begin{bmatrix}-d_3\\0\\d_1\end{bmatrix}e^{\mathbf{i}k\mathbf{x}\cdot\mathbf{d}}, \mathbf{d} = \begin{bmatrix}d_1\\0\\d_3\end{bmatrix}. \tag{3.38}$$

The decomposition (3.1) and (3.2) imply that the total field above the metal is the sum of the solution for the even and odd scattering problem under the incident wave

$$(\mathbf{E}^{\text{inc},(e)}(\mathbf{x}), \mathbf{H}^{\text{inc},(e)}(\mathbf{x})) = \frac{1}{2}(\mathbf{E}^{\text{inc},*}(\mathbf{x}^*), -\mathbf{H}^{\text{inc},*}(\mathbf{x}^*)), \tag{3.39}$$

and

$$(\mathbf{E}^{\text{inc},(o)}(\mathbf{x}), \mathbf{H}^{\text{inc},(o)}(\mathbf{x})) = -\frac{1}{2}(\mathbf{E}^{\text{inc},*}(\mathbf{x}^*), -\mathbf{H}^{\text{inc},*}(\mathbf{x}^*)) \tag{3.40}$$

respectively. In what follows, we only investigate the field amplification at the resonant frequencies for the even scattering problem. The amplification for the odd scattering problem can be dealt with similarly and the conclusion is similar. To this end, we introduce the reference field $(\mathbf{E}^{\text{r}}, \mathbf{H}^{\text{r}})$, which is the reflected field of the incident field (3.39) by the flat metallic slab without holes. Denote the solution to the even scattering problem by $(\mathbf{E}, \mathbf{H})$, then the T2T map defined in Theorem 3.1 can be written as

$$\gamma_T(\mathbf{H}) - \gamma_T(\mathbf{H}^{\text{r}}) = -\frac{2}{\mathbf{i}\omega\mu_0}\gamma_T\circ\mathcal{L}_k[\gamma_t(\mathbf{E})]. \tag{3.41}$$

By the same procedures performed in Section 3.3 and 3.4, for given angular momentum m and $p = 1\ldots, P$, we arrive at a non-homogeneous linear system in the form of (3.24)-(3.26) with the right-hand side given by

$$\left[f_{m,p}^{TE} \quad \left(g_{m,n',p}^{TE}\right)_{n'\in\mathbb{N}^*} \quad \left(g_{m,j',p}^{TM}\right)_{j'\in\mathbb{N}^*}\right]^T, \tag{3.42}$$

where

$$f_{m,p}^{TE} = \frac{\omega\mu_0}{2\mathbf{i}\lambda_{m,0,p}^N}(\gamma_T(\mathbf{H}^{\mathrm{r}}), \nabla_2\psi_{m,0,p}^N), \tag{3.43}$$

$$g_{m,n',p}^{TE} = \frac{\omega\mu_0}{2\mathbf{i}s_{m,n',p}^N\left(\lambda_{m,n',p}^N\right)^{1/4}}(\gamma_T(\mathbf{H}^{\mathrm{r}}), \nabla_2\psi_{m,n',p}^N), \tag{3.44}$$

$$g_{m,j',p}^{TM} = \frac{\omega\mu_0 s_{m,j',p}^D}{2\mathbf{i}\epsilon_r k^2\left(\lambda_{m,j',p}^D\right)^{1/4}}(\gamma_T(\mathbf{H}^{\mathrm{r}}), \mathrm{curl}_2\psi_{m,j',p}^D). \tag{3.45}$$

Note that $\gamma_T(\mathbf{H}^{\mathrm{r}})$ can be written as

$$\gamma_T(\mathbf{H}^{\mathrm{r}}) = \frac{\sqrt{\epsilon_0}}{\sqrt{\mu_0}}\begin{bmatrix} d_3 e^{-\mathbf{i}kd_3l/2+\mathbf{i}kd_1x_1} \\ 0 \\ 0 \end{bmatrix} = \begin{bmatrix} \frac{d_3 e^{-\mathbf{i}kd_3l/2}}{\mathbf{i}\omega\mu_0 d_1}\nabla_2 e^{\mathbf{i}kd_1 a\cos\theta} \\ 0 \end{bmatrix}, \tag{3.46}$$

for $d_1 \neq 0$, wherein $e^{\mathbf{i}kd_1 r\cos\theta}$ attains the Jacobi-Anger expansion (cf. eq. (3.89) in [12])

$$e^{\mathbf{i}kd_1 a\cos(\theta)} = \sum_{m=-\infty}^{\infty}\mathbf{i}^m J_m(kd_1a)e^{\mathbf{i}m\theta}. \tag{3.47}$$

The following asymptotic expansions hold:

$$f_{m,p}^{TE} = \frac{\sqrt{2\pi h_p}(\mathbf{i})^m d_3}{2d_1}e^{-\mathbf{i}kd_3l/2}a_p J_m(kd_1a_p) + \mathcal{O}(h^{3/2}), \tag{3.48}$$

$$g_{m,j',p}^{TE} = \mathcal{O}(h), \tag{3.49}$$

$$g_{m,n',p}^{TM} = 0. \tag{3.50}$$

For given $p = 1, \ldots, P$, we define

$$\mathbf{f}_m := \left(f_{m,p}^{TE}\right)_{p=1}^P, \ \mathbf{g}_{m,p} := \begin{bmatrix}\left(g_{m,n',p}^{TE}\right)_{n'\in\mathbb{N}^*} \\ \left(g_{m,j',p}^{TM}\right)_{j'\in\mathbb{N}^*}\end{bmatrix}, \ \mathbf{g}_m := \left(\mathbf{g}_{m,p}\right)_{p=1}^P.$$

Repeating the calculation in Section 3.5 gives the following finite-dimensional non-homogeneous system:

$$\left[\mathbf{D}_m - \mathbf{A}_m - \mathbf{R}_m\left(\mathbf{I}_{2P} - \mathbf{B}_m\right)^{-1}\mathbf{C}_m\right]\mathbf{d}_m = \mathbf{f}_m + \mathbf{R}_m\left(\mathbf{I}_{2P} - \mathbf{B}_m\right)^{-1}\mathbf{g}_m. \tag{3.51}$$

THEOREM 3.6. *Assume $0 < d_1 < 1$ and the incident wavenumber k is chosen as the real part of* (3.32) *or* (3.33)*. Then for the even scattering problem with incident field* (3.39)*, the total field inside the annual holes G^h has the following asymptotic*

$$\|\mathbf{E}\|_{H(\mathrm{curl},\mathrm{G^h})} = \mathcal{O}(h^{-\frac{1}{2}}) \text{ and } \|\mathbf{H}\|_{H(\mathrm{curl},\mathrm{G^h})} = \mathcal{O}(h^{-\frac{1}{2}}). \tag{3.52}$$

Proof. Since the imaginary parts of (3.32) and (3.33) are at least of order $\mathcal{O}(h^{-1})$, at the resonant frequency, Cramer's rule can be applied to (3.51) to show $\mathbf{d}_m = \mathcal{O}(h^{-1/2})$. For a given $p = 1, \ldots, P$, we define

$$\mathbf{c}_{m,p} := \begin{bmatrix} \mathbf{c}_{m,p}^{TE} \\ \mathbf{c}_{m,p}^{TM} \end{bmatrix}, \ \mathbf{c}_m := (\mathbf{c}_{m,p})_{p=1}^{P}.$$

Then $\mathbf{c}_m$ can be obtained as follows:

$$\mathbf{c}_m = (\mathbf{I}_{2P} - \mathbf{B}_m)^{-1} (\mathbf{C}_m \mathbf{d}_m + \mathbf{g}_m) = \mathcal{O}(1). \tag{3.53}$$

By recovering the Fourier coefficients in (3.15)-(3.16) from (3.27) and (3.28), and utilizing the asymptotic expansions of the Fourier modes in Theorem 2.4 derived in Appendix A and B of [28], we arrive at the desired expansion (3.52). ∎

4. Super-resolution imaging. In this section, we introduce and validate the super-resolution imaging framework. We first formulate the imaging problem using the Born approximation for weak scatterers and analyze how the high spatial-frequency information of the sample is encoded in the scattered field after the interaction. We then present an inversion algorithm to reconstruct the sample from the far-field measurement and conduct numerical examples to demonstrate the effectiveness of the imaging approach.

4.1. Born approximation for the imaging model. As shown in Figure 2, the substrate and sample are placed on the top of the metallic slab in the imaging setup. An oblique incident field is applied from below and the scattered field is collected on the far-field detector plane above the sample. Let $\mathbf{E}^{\text{tran}}$ be the transmitted electric field generated through annular holes shown in Figure 1, then the scattered field induced by the substrate and the imaging sample satisfies

$$\text{curlcurl}\mathbf{E}^{\text{sca}} - k^2(1+q)\mathbf{E}^{\text{sca}} = k^2 q \mathbf{E}^{\text{tran}}, \qquad \text{in } \mathbb{R}^3 \backslash \overline{\Omega}_M, \tag{4.1}$$

$$\boldsymbol{\nu} \times \mathbf{E}^{\text{sca}} = 0, \qquad \text{on } \partial\Omega_M. \tag{4.2}$$

We assume that both the substrate and the sample are thin with volume $V_q \ll 1$, as such they can be treated as weak scatterers. Let Ω_B denote the bounded region enclosed by $\partial\Omega_M$ and two semi-spherical surfaces centered at the origins of the upper and lower annular apertures, and Γ_0 denote $\partial\Omega_M \cap \partial\Omega_B$. We apply the Helmholtz decomposition introduced in Lemma 2.3 for $\mathbf{E}^{\text{sca}} \in H_{\Gamma_0}(\text{curl}, \Omega_B)$ and $q\mathbf{E}^{\text{tran}}/(1+q) \in [L^2(\Omega_B)]^3$, in which $A := k^2(1+q)$ and the inclusion map from $H_{\Gamma_0}(\text{curl}, \text{div}_A 0, \Omega_B)$ to $[L^2(\Omega_B)]^3$ is compact (cf. Corollary B.5 in [18]). Following the energy estimate used in [36], we have the following estimation for the scattered field:

THEOREM 4.1. *Assume that* $0 < c_1 < k^2(1+q(\mathbf{x})) < c_2$ *for constants* c_1 *and* c_2. *If the volume* $V_q \ll 1$, *then the scattering problem* (4.1)-(4.2) *attains a unique solution and there holds:*

$$\|\mathbf{E}^{\text{sca}}\|_{H_{\Gamma_0}(\text{curl},\Omega_B)} \lesssim \|q\mathbf{E}^{\text{tran}}\|_{[L^2(\Omega_B)]^3}. \tag{4.3}$$

The above theorem leads to the following Born's approximation (cf. Chapter XIII in [6]) for the scattering problem (4.1)-(4.2):

$$\text{curlcurl}\mathbf{E}^{\text{sca}} - k^2\mathbf{E}^{\text{sca}} = k^2 q \mathbf{E}^{\text{tran}}, \qquad \text{in } \mathbb{R}^3 \backslash \overline{\Omega}_M, \tag{4.4}$$

$$\boldsymbol{\nu} \times \mathbf{E}^{\text{sca}} = 0, \qquad \text{on } \partial\Omega_M. \tag{4.5}$$

Define the half-space Green's function

$$\widetilde{\mathbf{G}}_k(\mathbf{x},\mathbf{x}') := \mathbf{G}_k(\mathbf{x},\mathbf{x}') - \mathbf{G}_k^*(\mathbf{x},\mathbf{x}'^{,*}), \tag{4.6}$$

where $\mathbf{G}_k(\cdot,\cdot)$ denotes the free-space dyadic Green's function in $\mathbb{R}^3$, and $\mathbf{x}'^{,*}$ denotes the reflection of $\mathbf{x}'$ with respect to the plane $x_3 = l/2$. For a vector field $\mathbf{E}$ in $\mathbb{R}^3$, we introduce the potential

$$\mathcal{G}_k[\mathbf{E}](\mathbf{x}') := \iiint_{\mathbb{R}^3} \mathbf{E}(\mathbf{x}) \cdot \widetilde{\mathbf{G}}_k(\mathbf{x},\mathbf{x}')dv(\mathbf{x}). \tag{4.7}$$

Then $\mathbf{E}^{\mathrm{sca},q}$ can be expressed as

$$\mathbf{E}^{\mathrm{sca},q}(\mathbf{x}')=k^2\mathcal{G}_k[q\mathbf{E}^{\mathrm{tran}}](\mathbf{x}') - 2\mathcal{M}_k[\gamma_t(\mathbf{E}^{\mathrm{sca},q})](\mathbf{x}') \approx k^2\mathcal{G}_k[q\mathbf{E}^{\mathrm{tran}}](\mathbf{x}'),$$

where we neglect the field arising from the induced current over the tiny hole apertures that are negligibly small.

Assume that $\mathbf{E}^{\mathrm{sca},q}(\mathbf{x}')$ is measured on a far-field plane above the sample with a distance $x_3' = d$. The imaging problem seeks to reconstruct the sample function $q(\mathbf{x})$ from the measurement $\mathbf{E}^{\mathrm{sca},q}(\cdot,d)$.

4.2. Analysis of image resolution. We show that $\mathbf{E}^{\mathrm{sca},q}$ in the far-field detector plane carries the high spacial-frequency information of $q(\mathbf{x})$ if $\mathbf{E}^{\mathrm{tran}}(\mathbf{x})$ osscillates on a subwavelength scale. To this end, we define $\boldsymbol{\xi} := (\xi_1,\xi_2)$ and

$$\mathbf{M}_k(\boldsymbol{\xi}) = \frac{\mathbf{i}}{4\pi\sqrt{k^2-|\boldsymbol{\xi}|^2}}\left(\mathbf{I} + \frac{1}{k^2}\begin{bmatrix} -\xi_1^2 & -\xi_1\xi_2 & \xi_1\sqrt{k^2-|\boldsymbol{\xi}|^2} \\ -\xi_1\xi_2 & -\xi_2^2 & \xi_2\sqrt{k^2-|\boldsymbol{\xi}|^2} \\ \xi_1\sqrt{k^2-|\boldsymbol{\xi}|^2} & \xi_2\sqrt{k^2-|\boldsymbol{\xi}|^2} & -(k^2-|\boldsymbol{\xi}|^2)\end{bmatrix}\right).$$

THEOREM 4.2. *$\mathbf{E}^{\mathrm{sca},q}$ has the following approximation*

$$\begin{aligned}\mathbf{E}^{\mathrm{sca},q}(\mathbf{x}')\approx& k^2\int_{\mathbb{R}}\iint_{\mathbb{R}^2} \widehat{q\mathbf{E}^{\mathrm{tran}}}(\boldsymbol{\xi},x_3)\cdot\mathbf{M}_k(\boldsymbol{\xi})e^{\mathbf{i}(x_1'\xi_1+x_2'\xi_2)}e^{\mathbf{i}\sqrt{k^2-|\boldsymbol{\xi}|^2}(x_3'-x_3)}d\boldsymbol{\xi}dx_3 \\ &+ k^2\int_{\mathbb{R}}\iint_{\mathbb{R}^2} \widehat{q\mathbf{E}^{\mathrm{tran}}}(\boldsymbol{\xi},x_3)\cdot\mathbf{M}_k^*(\boldsymbol{\xi})e^{\mathbf{i}(x_1'\xi_1+x_2'\xi_2)}e^{\mathbf{i}\sqrt{k^2-|\boldsymbol{\xi}|^2}(x_3'+x_3-l)}d\boldsymbol{\xi}dx_3\end{aligned} \tag{4.8}$$

where $\widehat{\cdot}$ denotes the Fourier transform over $\mathbb{R}^2$.

Proof. We first compute the Fourier transform of $\widetilde{\mathbf{G}}_k(\mathbf{x},\mathbf{x}')$ with respect to the the x_1, x_2 variables. Recall that $\mathbf{G}_k$ has the following expression (cf. Section 1.3.4 in [11]):

$$\mathbf{G}_k(\mathbf{x},\mathbf{x}') = \left(\mathbf{I} + \frac{1}{k^2}\nabla\nabla\right)\Phi_k(\mathbf{x},\mathbf{x}'), \tag{4.9}$$

where $\mathbf{I}$ is the identity operator and $\Phi_k(\mathbf{x},\mathbf{x}')$ satisfies

$$(\Delta + k^2)\Phi_k(\mathbf{x},\mathbf{x}') = -\delta(\mathbf{x}-\mathbf{x}'). \tag{4.10}$$

Applying the Fourier transform over x_1, x_2 on both sides of (4.10) yields

$$(k^2 - |\boldsymbol{\xi}|^2 + \partial_{x_3}^2)\widehat{\Phi}_k(\xi_1,\xi_2,x_3,\mathbf{x}') = -\frac{e^{-\mathbf{i}(x_1'\xi_1+x_2'\xi_2)}}{2\pi}\delta(x_3-x_3'). \tag{4.11}$$

Solving (4.11) leads to

$$\widehat{\Phi}_k(\xi_1,\xi_2,x_3,\mathbf{x}') = \frac{\mathbf{i}e^{\mathbf{i}\sqrt{k^2-|\boldsymbol{\xi}|^2}|x_3-x_3'|}}{4\pi\sqrt{k^2-|\boldsymbol{\xi}|^2}}e^{-\mathbf{i}(x_1'\xi_1+x_2'\xi_2)}, \tag{4.12}$$

and it follows that

$$\widehat{\mathbf{G}}_k(\boldsymbol{\xi},x_3,\mathbf{x}') = \mathbf{M}_k(\boldsymbol{\xi})e^{-\mathbf{i}(x_1'\xi_1+x_2'\xi_2)}e^{\mathbf{i}\sqrt{k^2-|\boldsymbol{\xi}|^2}(x_3'-x_3)}, \tag{4.13}$$

$$\widehat{\mathbf{G}}_k^*(\boldsymbol{\xi},x_3,\mathbf{x}'^{,*}) = \mathbf{M}_k^*(\boldsymbol{\xi})e^{-\mathbf{i}(x_1'\xi_1+x_2'\xi_2)}e^{\mathbf{i}\sqrt{k^2-|\boldsymbol{\xi}|^2}(x_3'+x_3-l)}. \tag{4.14}$$ ∎

We obtain (4.8) using the Parseval–Plancherel identity and (4.13) - (4.14).

The formula (4.8) implies only the information in $\{|\boldsymbol{\xi}| \le k\}$ of $\widehat{q\mathbf{E}^{\mathrm{tran}}}(\boldsymbol{\xi},x_3)$ can be detected on the far-field plane when $|d-l/2| \gg \lambda$. If $\mathbf{E}^{\mathrm{tran}}$ is locally a plane wave and q is separable such that

$$\mathbf{E}^{\mathrm{tran}} = \mathbf{E}_0 e^{\mathbf{i}(\kappa_1x_1+\kappa_2x_2+\kappa_3x_3)}, \quad q = q_a(x_1,x_2)q_b(x_3),$$

where $\kappa_1,\kappa_2,\kappa_3 \in \mathbb{R}$ and $\kappa_1^2+\kappa_2^2+\kappa_3^2 = k^2$, then

$$\widehat{q\mathbf{E}^{\mathrm{tran}}}(\boldsymbol{\xi},x_3) = \mathbf{E}_0\widehat{q_a}(\boldsymbol{\xi}-(\kappa_1,\kappa_2))q_b(x_3)e^{\mathbf{i}\kappa_3x_3}. \tag{4.15}$$

We deduce that the Fourier components of $\widehat{q_a}$ in the frequency band

$$\Omega(k,\kappa_1,\kappa_2) := \{\boldsymbol{\xi}-(\kappa_1,\kappa_2);\ |\boldsymbol{\xi}| \le k, \kappa_1^2+\kappa_2^2+\kappa_3^2 = k^2\} \tag{4.16}$$

can be recovered from the far-field measurement, and the image resolution is determined by the horizontal wave vector (κ_1,κ_2) of $\mathbf{E}^{\mathrm{tran}}$ for a fixed incident frequency.

By arranging a set of P annular holes within one wavelength, at the resonant frequencies, the transmitted field through the holes contains high spatial-frequency wave in the form of $\mathbf{E}_0e^{\mathbf{i}(\kappa_1x_1+\kappa_2x_2)-\kappa_3x_3}$ satisfying $\kappa_1^2+\kappa_2^2 \gg k^2$; See Figure 3 for an illustration. In light of (4.16), such an illumination pattern allows for recovering high Fourier components of the imaging sample, leading to a better image resolution.

4.3. Imaging Algorithm. We employ a set of frequencies $\{k_i\}_{i=1}^{N_1}$ near the real part of a complex-valued resonance for the incident wave, along with a set of rotation and translation transformations $\{T_j\}_{j=1}^{N_2}$ for the sample function q. By using the transmitted field $\mathbf{E}^{\mathrm{tran},i}$ through the holes as an illumination pattern, we collect the scattered field $\mathbf{E}^{\mathrm{sca},q}$ on the plane $x_3 = d$ when the sample is absent and present respectively. Here the transformations $\{T_j\}_{j=1}^{N_2}$ are deployed to maximize the interactions between the transmitted fields $\mathbf{E}^{\mathrm{tran},i}$ and the sample. Our reconstruction procedure for the sample function $q(\mathbf{x})$ is performed as follows:

1. Compute the transmitted field through the annular holes $\mathbf{E}^{\mathrm{tran},i}$ in (4.1) for each given k_i:
   - 1.1. Given the incidence, solve the linear system (3.51) to obtain the coefficients of the dominated modes on the aperture;
   - 1.2. Apply the formula (3.5) to compute $\mathbf{E}^{\mathrm{tran},i}$.
2. Discretize the integral operator (4.8) for $x_3' = d$ to obtain a linear mapping L^i from q to $\mathbf{E}^{\mathrm{sca},q}$ for each $\mathbf{E}^{\mathrm{tran},i}$.

3. Reconstruct q from the linear system

$$\begin{bmatrix} \vdots \\ L_i T_j \\ \vdots \end{bmatrix} q = \begin{bmatrix} \vdots \\ b^{\delta}_{i,j} \\ \vdots \end{bmatrix}, \tag{4.17}$$

where $b^{\delta}_{i,j}$ denotes the measured data with a noise level δ for each given k_i and T_j.

Let $\mathbf{L}$, q and $\mathbf{b}^{\delta}$ denote the matrix, the sample dielectric vector and the data vector in (4.17) respectively. The solution of (4.17) is obtained by solving the optimization problem

$$\min_{q\in\mathbb{R}^N} \|\mathbf{L}q - \mathbf{b}^{\delta}\|_2^2. \tag{4.18}$$

We apply the gradient-descent method to recover q, which is insensitive to the highly oscillatory noise in the measurement by using the smooth operator $\mathbf{L}^*\mathbf{L}$ in the gradient direction.

4.4. Numerical examples. We consider the subwavelength structure with ten annular holes being patterned in a metallic slab of thickness $l = 1$. The inner and outer radii of each hole are given by $a_p = 0.6p$ and $a_p(1 + h_p) = 0.6p + 0.1$ for $p = 1, \ldots, 10$. The relative electric permittivity inside the annular hole is chosen as $\epsilon_r = 25/9$. Let the incident wave be oriented along the direction $[\sqrt{3}/2, 0, 1/2]^T$, with the incident wavenumber given by the following five resonant frequencies in (3.32): $k_1 = k_{5,0,5} \approx 1.0479$, $k_2 = k_{6,0,6} \approx 1.0504$, $k_3 = k_{7,0,7} \approx 1.0523$, $k_4 = k_{8,0,8} \approx 1.0537$ and $k_5 = k_{9,0,9} \approx 1.0548$. We denote the approximate incident wavelength by $\lambda = 2\pi$.

The imaging sample attains a compact support $\mathbf{V}^{\text{sam}} := [-\sqrt{2}\pi, -\sqrt{2}\pi + \pi] \times [\sqrt{2}\pi - \pi, \sqrt{2}\pi] \times [\frac{l}{2} + 0.1, \frac{l}{2} + 0.3]$, which is discretized using a $40 \times 40 \times 4$ rectangular grid. In the numerical examples, we assume that the sample function $q = q_a(x_1, x_2)$ inside $\mathbf{V}^{\text{sam}}$. We use a set of rotations $\{T_j\}_{j=1}^{11}$, where each T_j represents a rotation by $j\pi/6$ radians for the sample. The far-field detector plane is positioned at a distance of 10λ above the metal, with the measurement region $\mathbf{V}^{\text{far}} := [-12\pi, 12\pi] \times [-12\pi, 12\pi] \times \{\frac{l}{2} + 20\pi\}$ that is discretized with a 120×120 rectangular grid.

EXAMPLE 4.3 (transmitted wave pattern). *We investigate the transmitted wave through by the subwavelength structure at the resonant frequencies. Figure 3 illustrates the electric field at a height of $x_3 = l/2 + 0.23$ when the incident wavenumber is k_3. It is clear that the wave oscillates on a subwavelength scale on the x_1x_2 plane.*

EXAMPLE 4.4 (super-resolution imaging). *We consider measurement data with 10% additive Gaussian random noise. The gradient descent method employed for reconstruction is terminated with a relative tolerance of 10^{-3}. The first and second row in Figure 4 display the true sample images and the reconstructed images obtained using our imaging approach respectively. It is observed that a resolution of $\lambda/20$ is achieved for the reconstruction. For comparison, in the third row of Figure 4, we also plot reconstructed images if the resonant subwavelength structure is absent.*

5. Conclusion. In this work, we have investigated the resonances for an array of subwavelength annular holes and presented a new super-resolution imaging method using the resonant structure. By extending the multiscale framework developed in [28] for the single hole to an array of holes, we obtain the asymptotic expansion for the complex-valued resonances and analyzed the field amplification at the resonant

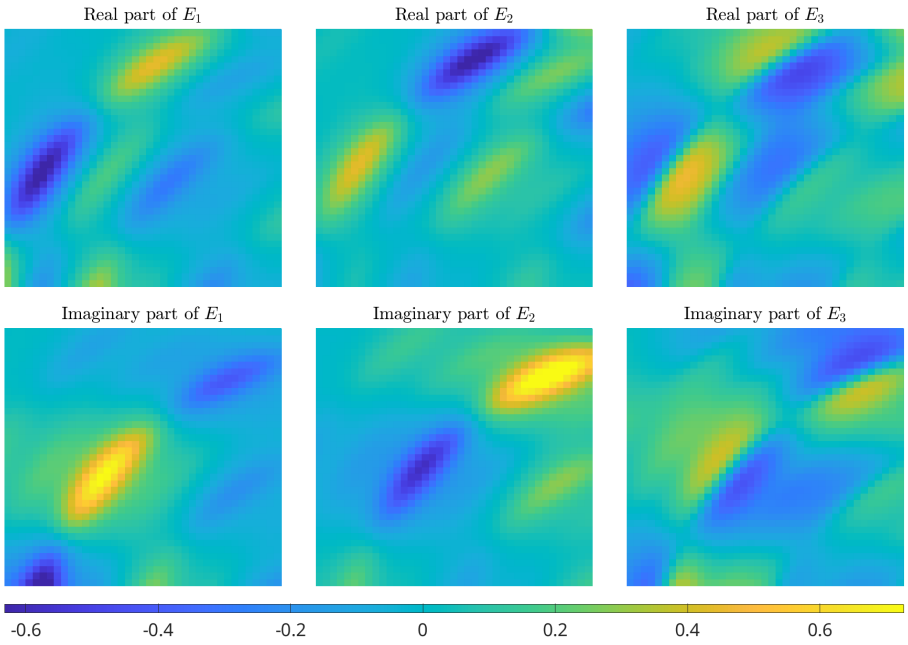

FIG. 3. *The transmitted electric field in the region* $[-\sqrt{2}\pi, -\sqrt{2}\pi+\pi]\times[\sqrt{2}\pi-\pi, \sqrt{2}\pi]$ *over the plane* $x_3 = \times\{l/2+0.23\}$. *The corresponding incident plane wave is applied below the subwavelength structure with the resonant frequency* $k_3 \approx 1.0523$.

frequencies quantitatively. The super-resolution imaging approach uses the highly oscillatory resonant transmitted field as the illumination pattern, which probes the high spatial frequency information of the sample and improves the resolution of the image significantly. Furthermore, the reconstruction algorithm for solving the underlying imaging problem is stable against noise by using low-frequency far-field data. The study sheds light on the use of electromagnetic resonant scattering for optical imaging. Mathematical modeling and computational tools can be developed to investigate resonances in more complex subwavelength structure and their capabilities to further improve the image resolution.

REFERENCES

[1] H. Ammari and H. Zhang, *Effective medium theory for acoustic waves in bubbly fluids near minnaert resonant frequency*, SIAM Journal on Mathematical Analysis, 49 (2017), pp. 3252–3276.

[2] H. M. Ammari and H. Zhang, *A mathematical theory of super-resolution by using a system of sub-wavelength helmholtz resonators*, Communications in Mathematical Physics, 337 (2015), pp. 379–428.

[3] J.-F. Babadjian, E. Bonnetier, and F. Triki, *Enhancement of electromagnetic fields caused by interacting subwavelength cavities*, Multiscale Model. Simul., 8 (2010), pp. 1383–1418.

[4] G. Bao and P. Li, *Near-field imaging of infinite rough surfaces*, SIAM Journal on Applied Mathematics, 73 (2013), pp. 2162–2187.

[5] G. Bao and J. Lin, *Near-field imaging of the surface displacement on an infinite ground plane*, Inverse Probl. Imaging, 7 (2013), pp. 377–396.

[6] M. Born, E. Wolf, A. B. Bhatia, P. C. Clemmow, D. Gabor, A. R. Stokes, A. M. Taylor, P. A. Wayman, and W. L. Wilcock, *Principles of Optics: Electromagnetic Theory of*

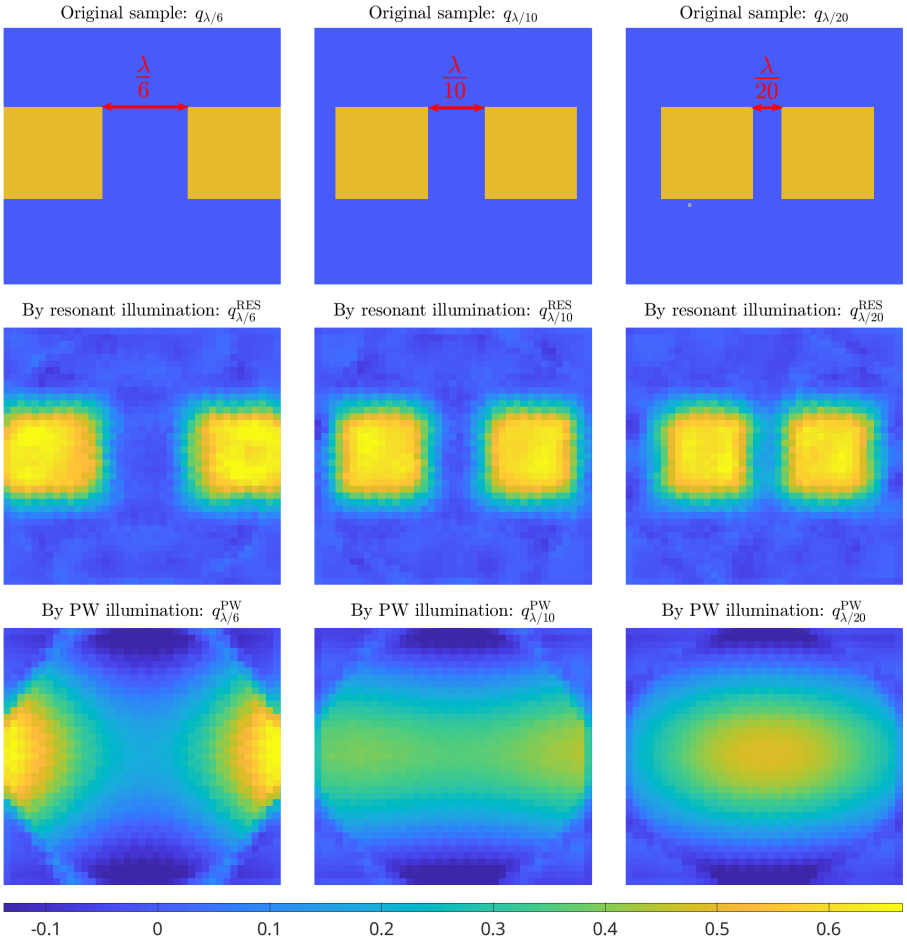

FIG. 4. *The first row displays the true images for the sample function* $q_a(x_1, x_2)$ *over the region* $[-\sqrt{2}\pi, -\sqrt{2}\pi + \pi] \times [\sqrt{2}\pi - \pi, \sqrt{2}\pi]$. *The distances between two objects are* $\lambda/6$, $\lambda/10$ *and* $\lambda/20$, *respectively. The second row presents the reconstructed images obtained by our imaging approach, and the third row displays the reconstructed images if the subwavelenth structure is absent.*

Propagation, Interference and Diffraction of Light, Cambridge University Press, 7 ed., 1999.

[7] R. Brandão, J. R. Holley, and O. Schnitzer, *Boundary-layer effects on electromagnetic and acoustic extraordinary transmission through narrow slits*, Proc. A., 476 (2020), p. 20200444.

[8] P. S. Carney, V. A. Markel, and J. C. Schotland, *Near-field tomography without phase retrieval*, Physical review letters, 86 (2001), p. 5874.

[9] P. S. Carney and J. C. Schotland, *Inverse scattering for near-field microscopy*, Applied Physics Letters, 77 (2000), pp. 2798–2800.

[10] P. S. Carney and J. C. Schotland, *Three-dimensional total internal reflection microscopy*, Optics Letters, 26 (2001), pp. 1072–1074.

[11] W. Chew, *Waves and Fields in Inhomogeneous Media*, IEEE Press, 1995.

[12] D. Colton and R. Kress, *Inverse Acoustic and Electromagnetic Scattering Theory*, Springer Cham, 3rd ed., 2013.

[13] R. Dautray and J.-L. Lions, *Mathematical Analysis and Numerical Methods for Science and Techonology Volume 3: Spectral Theory and Applications*, Springer, 2000.

[14] T. W. Ebbesen, H. J. Lesec, T. Thio, and P. A. Wolff, *Extraordinary optical transmission through sub-wavelength hole arrays*, Nature, 391 (1998), pp. 667–669.
[15] M. Fatima and L. Lin, *Scattering resonances for a three-dimensional subwavelength hole*, Partial Differential Equations and Applications, 2 (2021), p. 56.
[16] M. G. Gustafsson, *Surpassing the lateral resolution limit by a factor of two using structured illumination microscopy*, Journal of microscopy, 198 (2000), pp. 82–87.
[17] A. Hartschuh, *Tip-enhanced near-field optical microscopy*, Handbook of Spectroscopy: Second, Enlarged Edition, (2014), pp. 1585–1610.
[18] C. Hazard and M. Lenoir, *On the solution of time-harmonic scattering problems for maxwell's equations*, SIAM J. Math. Anal., 27 (1996), pp. 1597–1630.
[19] B. Hecht, B. Sick, U. P. Wild, V. Deckert, R. Zenobi, O. J. Martin, and D. W. Pohl, *Scanning near-field optical microscopy with aperture probes: Fundamentals and applications*, The Journal of Chemical Physics, 112 (2000), pp. 7761–7774.
[20] R. Heintzmann and T. Huser, *Super-resolution structured illumination microscopy*, Chemical reviews, 117 (2017), pp. 13890–13908.
[21] R. J. Holley and O. Schnitzer, *Extraordinary transmission through a narrow slit*, Wave Motion, 91 (2019), p. 102381.
[22] G. Huszka and M. A. Gijs, *Super-resolution optical imaging: A comparison*, Micro and Nano Engineering, 2 (2019), pp. 7–28.
[23] A. Kirsch and F. Hettlich, *The Mathematical Theory of Time-Harmonic Maxwell's Equations*, Springer Cham, 2014.
[24] M. Lanoy, R. Pierrat, F. Lemoult, M. Fink, V. Leroy, and A. Tourin, *Subwavelength focusing in bubbly media using broadband time reversal*, Phys. Rev. B, 91 (2015), p. 224202, https://doi.org/10.1103/PhysRevB.91.224202, https://link.aps.org/doi/10.1103/PhysRevB.91.224202.
[25] F. Lemoult, M. Fink, and G. Lerosey, *Acoustic resonators for far-field control of sound on a subwavelength scale*, Phys. Rev. Lett., 107 (2011), p. 064301, https://doi.org/10.1103/PhysRevLett.107.064301, https://link.aps.org/doi/10.1103/PhysRevLett.107.064301.
[26] G. Lerosey, J. Rosny, A. Tourin, and M. Fink, *Focusing beyond the diffraction limit with far-field time reversal*, Science (New York, N.Y.), 315 (2007), pp. 1120–2, https://doi.org/10.1126/science.1134824.
[27] Y. Liang and J. Zou, *Acoustic scattering and field enhancement through a single aperture*, arxiv: 2011.05887, (2020).
[28] J. Lin, W. Lu, and H. Zhang, *Mathematical theory for electromagnetic scattering resonances and field enhancement in a subwavelength annular gap*, Multiscale Model. Simul., 21 (2023), pp. 1012–1052.
[29] J. Lin, P. Shipman, Stephen, and H. Zhang, *A mathematical theory for fano resonance in a periodic array of narrow slits*, SIAM J. Appl. Math., 80 (2020), pp. 2045–2070.
[30] J. Lin and H. Zhang, *Scattering and field enhancement of a perfect conducting narrow slit*, SIAM J. Appl. Math., 77 (2017), pp. 951–976.
[31] J. Lin and H. Zhang, *Scattering by a periodic array of subwavelength slits I: Field enhancement in the diffracttion regime*, Multiscale Model. Simul., 16 (2018), pp. 922–953.
[32] J. Lin and H. Zhang, *Scattering by a periodic array of subwavelength slits II: Surface bound states, total transmission, and field enhancement in homegenization regimes*, Multiscale Model. Simul., 16 (2018), pp. 954–990.
[33] J. Lin and H. Zhang, *Superresolution imaging via subwavelength hole resonances*, Phys. Rev. Appl., 14 (2020), p. 034066.
[34] W. Lu, W. Wang, and J. Zhou, *A fourier matching method for analyzing resonances in a sound-hard slab with subwavelength holes*, CSIAM Trans. Appl. Math., 5 (2024), pp. 234–263.
[35] W. Mclean, *Strongly Elliptic System and Boundary Integral Equations*, Cambridge University, 2000.
[36] P. Monk, *Finite Element Methods for Maxwell's Equations*, Clarendon Press, 2003.
[37] L. Novotny and S. J. Stranick, *Near-field optical microscopy and spectroscopy with pointed probes*, Annu. Rev. Phys. Chem., 57 (2006), pp. 303–331.
[38] S. G. Rodrigo, F. de Leon-Perez, and L. Martin-Moreno, *Extraordinary optical transmission: fundamentals and applications*, Proceedings of the IEEE, 104 (2016), pp. 2288–2306.
[39] W. Rudin, *Functional Analysis*, McGraw-Hill Science, 2nd ed., 1991.
[40] J. Zhou and W. Lu, *Numerical analysis of resonances by a slab of subwavelength slits by fourier-matching method*, SIAM J. Numer. Analy., 59 (2021), pp. 2106–2137.